# SCATTERING OF ATOMS BY MOLECULES ADSORBED AT SOLID SURFACES

By

ZAIDA PARRA

A DISSERTATION PRESENTED TO THE GRADUATE SCHOOL
OF THE UNIVERSITY OF FLORIDA IN
PARTIAL FULFILLMENT OF THE REQUIREMENTS
FOR THE DEGREE OF DOCTOR OF PHILOSOPHY

UNIVERSITY OF FLORIDA

1988

UNIVERSITY OF FLORIDA LIBRARIES

TO
GILBERTO CARLOS
AND
CAMILO

ACKNOWLEDGEMENTS

I would like to thank my adviser, Professor David A. Micha, for his invaluable ideas, guidance and support during the development of this work. Also, I wish to extend my appreciation to the professors of the Quantum Theory Project who have contributed to my education and made the Quantum Theory Project such a stimulating and enriching environment. I would particularly like to express my gratitude toward Professor Per-Olov Löwdin who made possible my participation in the 1983 Summer School in Quantum Theory in Uppsala, Sweden.

My deepest appreciation is to my husband Ray Little, for his support and patience during these years of studies.

Finally, my thanks go to Rohin Bastenzi for her help in the typing of this dissertation.

TABLE OF CONTENTS

ACKNOWLEDGEMENTS ... iii

ABSTRACT ... iv

CHAPTERS

1. INTRODUCTION ... 1

2 COLLISIONAL TIME-CORRELATION FUNCTION APPROACH TO ENERGY TRANSFER ... 7

2.1 Many-Body Approach ... 8
2.2 The Impulse Approximation ... 12
2.3 Application to Scattering by Adsorbates ... 16

3 VIBRATIONAL FREQUENCIES AND NORMAL MODES OF MOLECULES ADSORBED ON SURFACES ... 19

3.1 Cluster Models and Force Fields ... 21
3.2 Normal Modes Analyses ... 28
3.3 Numerical Results for CO on Ni(001) ... 33

4 ENERGY TRANSFER INTO MOLECULAR ADSORBATES ... 46

4.1 The Vibrational Correlation Function ... 47
4.2 Short Time Expansion ... 50
4.3 Statistical Model for Single and Double Collisions ... 51

5 GAS-ADSORBATE INTERACTION POTENTIALS EFFECTIVE DIFFERENTIAL CROSS SECTIONS ... 57

5.1 Atom (Ion)-Adsorbate Interaction Potentials ... 58
5.2 Effective Classical Differential Cross-Sections ... 80

6 VIBRATIONAL ENERGY TRANSFER IN HYPERTHERMAL COLLISIONS OF He AND $Li^+$ WITH CO ADSORBED ON Ni(001) ... 94

6.1 Double Differential Cross-Sections for the System He/CO Ni(001) ... 94
6.2 Double Differential Cross-Sections for the System $Li^+$/CO Ni(001) ... 97

7 SUMMARY AND CONCLUSIONS ... 146

APPENDICES

A COEFFICIENTS FOR TRANSFORMATION $\underset{\sim}{R}=\underset{\sim}{AX}$ ... 155
B SYMMETRY ADAPTED COORDINATES ... 158
C COEFFICIENTS FOR TRANSFORMATION $\underset{\sim}{Q}=\underset{\sim}{CX}$ ... 159

REFERENCES ... 162

BIOGRAPHICAL SKETCH ... 166

Abstract of Dissertation Presented to the Graduate School of the University of Florida in Partial Fulfillment of the Requirements for the Degree of Doctor of Philosophy

SCATTERING OF ATOMS BY MOLECULES ADSORBED AT SOLID SURFACES

By

ZAIDA PARRA

August, 1983

Chairman: David A. Micha
Major Department: Chemistry

The formalism of collisional time-correlation functions, appropriate for scattering by many body targets, is implemented to study energy transfer in the scattering of atoms and ions from molecules adsorbed on metal surfaces.

Double differential cross sections for the energy and angular distributions of atoms and ions scattered by a molecule adsorbed on a metal surface are derived in the limit of impulsive collisions and within a statistical model that accounts for single and double collisions. They are found to be given by the product of an effective cross-section that accounts for the probability of deflection into a solid angle times a probability per unit energy transfer.

A cluster model is introduced for the vibrations of an adsorbed molecule which includes the molecular atoms, the surface atoms binding the molecule, and their nearest neighbors.

The vibrational modes of CO adsorbed on a Ni(001) metal surface are obtained using two different cluster models to represent the on top and bridge-bonding situations

A short-time expansion is introduced for the slow modes of the target, which leads to Gaussian distributions of the energy transferred into the slow modes

A He/OC-Ni(001) potential is constructed from a strongly repulsive potential of He interacting with the oxygen atom in the CO molecule and a van der Waals attraction accounting for the He interaction with the free Ni(001) surface. A potential is also presented for the $Li^+$/OC Ni(001) where a coulombic term is introduced to account for the image force.

Trajectory studies are performed in three dimensions to obtain effective classical cross-sections for the He/OC-Ni(001) and $Li^+$/OC Ni(001) systems. These cross-sections are then used to calculate the double differential cross sections per unit solid angle and energy transfer for the same systems. Results for the double differential cross-sections are presented as functions of scattering angles, energy transfer and collisional energy. Temperature dependence results are also analyzed. Extensions of the approach and inclusion of effects such as anharmonicity, collisions at lower energies, and applications of the approach to higher coverages are discussed.

# CHAPTER 1
# INTRODUCTION

In the past few years, there has been an increasing interest in the study of metal surfaces by a wide variety of experimental techniques. An important aspect of metal surfaces is their ability to effectively adsorb atoms and molecules, leading to chemisorption surface reactions, or catalysis.

The experimental study of the vibrational modes of atoms and molecules adsorbed at surfaces has proved to be a powerful means of deriving information about changes in molecular bonding which occur during chemisorption processes and also on the preferred adsorption sites (Rocca et al., 1986).

Vibrational spectra of adsorbates have been observed with infrared reflection spectroscopy (IRS) and with low-energy electron scattering (EELS). These techniques are in practice sensitive only to the dipole-active high frequency modes of vibration, which correspond to either intrinsic vibrations of the free molecule or to the high frequency vibration of the molecule perpendicular to the surface. A further class of low frequency modes, the hindered rotations and translations parallel to the surface, also exists but their observation is prevented by the instrumental resolution in EELS and the limited spectral range and sensitivity of IRS. A technique which is in principle an ideal method for studying these vibrations is inelastic atom scattering spectroscopy. It also has the capability to observe the dynamics of surface adsorbate layers and is

sensitive to very small amounts of adatoms on smooth metal substrates and can, therefore, give information about isolated adatoms (Gadzuk, 1987)

Several articles have appeared on experimental aspects of scattering by adsorbates. Systems which have been studied by neutral atom scattering include, among others, He with either O or CO on Ni(001) (Ibañez et al., 1983) and He with CO on Pt(111). In the latter system cross sections have been measured as a function of the velocity of the incident He atoms and the angle of incidence (Poelsema et al., 1983) and as a function of scattering angle and momentum transfer (Lahee et al., 1987)

All of the experiments with neutral atoms have been done with energies in the thermal regime. Ions have also been used as probes in experiments of scattering by adsorbates. In one of the pioneer works in the area (Huipke, 1975), energy and angular distributions of $Li^+$ ions scattered by clean W(110) surfaces and by adsorbates, such as $O_2$ and CO, were measured for beam energies between 2 and 20 eV

Scattering intensities in the systems $Li^+$-O/Ni(110) and $He^+$-O/Ni(110) have been measured as a function of the scattering angles and relative energies of the ions (Englert et al., 1983). Recently, measurements on angle and energy distributions of $K^+$ ions scattered from W(110) in the energy range of 12 to 100 eV have been published (Tenner et al., 1986). These measurements have been done at normal incidence.

In general, most of the theoretical approaches to the problem of scattering by adsorbates have concentrated on elastic scattering. Furthermore, since a detailed theoretical treatment is virtually impossible to accomplish because of the computing time and memory

required, approximate schemes are a necessity. Several approaches to the scattering of atoms with thermal energies by adsorbates have been based on extensions of methods which have been useful in the description of scattering by clean surfaces. The general theory of atom scattering in the eikonal approximation has been extended to scattering by overlayers (Levi, 1982). In this theory the motion of the adsorbate is assumed to be separated from the motion of the substrate and does not contain information on the site occupied by the adsorbate. A theory for scattering by adatoms at low coverage has been presented (Jansson et al., 1984). Here the surface is considered to be a hard wall and the cross-section for the isolated adatom is simply given by an effective scattering amplitude obtained by subtracting the scattering amplitude of a hard wall from the gas-phase scattering amplitude for the adatom. This theory has been applied to the system He-OC/Pt using the distorted wave Born approximation (Liu and Gunthaler, 1987), and the cross-sections have been calculated from the formalism of close coupled equations. However, the possibility of inelastic scattering increases the computational complexity of the problem. Quantal approaches have been based on wavepackets (Gerber et al., 1984) and on multiple-collision expansions (Singh et al., 1986). With a few exceptions (Villalonga and Rabitz, 1986) theoreticians have considered only elastic Bragg scattering which gives information on the structure of adsorbate covered surfaces or the elastic component of diffuse scattering from adsorbates. However, the inelastic scattering is of great interest because it involves the excitation of surface phonons and the vibrational modes of the adsorbed molecule.

When an atom collides with a molecule adsorbed on a metal surface, kinetic energy can be transferred into one of the infinite number of vibrational modes of the target. Consequently, one is not interested in the state-to-state cross-sections familiar in scattering by isolated molecules, but instead one wants double differential cross-sections, per unit of solid angle and of energy transfer. Furthermore, the quantities of experimental interest are averages of these cross-sections with respect to statistical distributions of target states for the given surface temperature.

The purpose of this dissertation is to present a model of energy transfer for the scattering of atoms and ions from diatomic molecules adsorbed on a metal surface.

Recent experiments have shown (Berndt et al., 1987) that information on the type of interaction between atoms and adsorbed molecules as well as on the vibrational modes of adsorbed molecules can be obtained from isolated adsorbates. Therefore, we are interested in a model which could be applicable to low coverages, and in a simple theory which could provide insights into the type of interactions and also be able to predict trends in the energy and angular distributions of the scattered particles.

Standard treatments of molecular collisions, based on target state expansions, are not convenient because excited target states are usually unknown. Instead, one can use the formalism of collisional time-correlation functions (Micha, 1986) which is appropriate for scattering by many-body targets and includes statistical averages.

For hyperthermal collisions, the interaction is dominated by strong short range repulsive forces and lasts a short time compared

with the periods of internal motions of the target, so that an impulsive model is appropriate. Furthermore, as long as the projectile is light compared with target atoms, only a single collision occurs with the adsorbate before the projectile flies away. These two features lead to a simple expression for the time correlation, which can then be obtained analytically from the normal vibrational modes of the target.

The vibrations of an adsorbed molecule can be modelled by a cluster which includes the molecular atoms, the surface atoms binding the molecule, and their nearest neighbors. The normal modes of the target can be grouped into two sets, one with high frequencies (fast modes) similar to those of the isolated molecule and the other with low frequencies (slow modes) characteristic of the surface vibrations.

When the target involves slow modes, one can approximate the time-correlation functions by short time expansions which lead to Gaussian distributions of the energy transferred into the slow modes.

The present work is presented here as follows: In Chapter 2 the formalism of collision time-correlation functions is presented together with expressions for the differential cross-sections within the impulsive model, and its application to scattering by adsorbates. Two models are developed in Chapter 3 to represent on-top and bridge adsorption sites of a CO molecule adsorbed on Ni(001). Depending on the angle of scattering, the interaction between the projectile and the target may involve only the single collision with the adsorbate, or that followed by a collision with the solid surface. In Chapter 4 we develop a statistical model to calculate contributions of double collisions to the cross sections. In order to calculate the double

differential cross sections, one first needs to obtain effective classical cross-sections. We use the facts that the potentials of the separate adsorbates do not overlap and that the translational wavelength of the projectile is much shorter than the range of the intermolecular potential. Thus translation of the projectile is obtained by a classical trajectory. In Chapter 5 the interaction potential for the systems $Li^+$-OC/Ni(001) and He-OC/Ni(001) are constructed and trajectory studies are performed to obtain the effective classical cross-sections. In Chapter 6 results of double differential cross-sections for the systems $Li^+$-OC/Ni(001) and He-OC/Ni(001) are given as a function of energy transfer and scattering angles. Finally, in Chapter 7 the advantages and disadvantages of the approach are presented together with some suggestions on possible improvements of the approach.

# CHAPTER 2
# COLLISIONAL TIME-CORRELATION FUNCTION APPROACH TO ENERGY TRANSFER

When an atom is scattered by a target, energy can be transferred from the projectile into the target or out of the target to the projectile. The amount of energy transferred is determined to a large extent by the intramolecular dynamics of the target, therefore it is expected that atomic motions within the target will place certain constraints on the process.

The theoretical description of the energy transfer between atoms and extended targets can be done using classical, semiclassical or quantum mechanical methods. The quantum mechanical methods are usually based on expansions in target states but are computationally impractical and costly due to the large number of energetically accessible levels of the target. An alternative approach which takes into account the quantal nature of the target motion, but avoids expansions in target states has been developed (Miller, 1979a) and used in the study of atom-polyatomic collisions (Miller, 1979b). In such an approach the target is described as a many-atom system and atom-pair correlation functions of the target play an important role in the description of the process. In this chapter we review the main features of this many body theory in its exact form and then discuss a simplification of the approach, namely the impulse approximation, which makes the approach more tractable for its application to the scattering of atoms by adsorbates.

## 2.1 Many Body Approach

The type of process we are interested can in general be described by

$$A(E_i) + X(\nu) \rightarrow A(E_f) + X(\nu') ,$$

where A denotes an atom with an initial kinetic energy $E_i$ and X represents a many atom system, e.g., an adsorbate on a metal surface, in an initial internal state $\nu$. During the collision an amount of energy $\varepsilon$ is transferred between them, promoting X to a final internal state $\nu'$ and leaving A with a final kinetic energy $E_f$.

In the laboratory frame, with $\vec{R}_A$ denoting the position of the projectile the Hamiltonian of the projectile is simply its kinetic energy

$$H_A = -\frac{\hbar^2}{2m_\theta}\vec{\nabla}^2_{\vec{R}_A} , \tag{2.1}$$

and the internal Hamiltonian $H_X$ for the target may be written as

$$H_X = \sum_\theta \frac{\hbar^2}{2m_\theta}\vec{\nabla}^2_{\vec{r}_\theta} + V_X(\vec{r}^X) , \tag{2.2}$$

where $\vec{r}_\theta$ is the position of atom $\theta$ and $\vec{r}^X = \{\vec{r}_\theta\}$ the collection of these vectors.

In the coordinate system fixed to the center of mass of the pair (A,X), the system Hamiltonian is given by

$$H = H_0 + V , \tag{2.3a}$$

where

$$H_0 = K + H_{\vec{r}^X} \tag{2.3b}$$

Here K is the operator for the kinetic energy of the relative motion given by

$$\bar{K} = -\frac{\hbar^2}{2M}\nabla^2_{\vec{R}} \quad , \tag{2.3c}$$

where $\vec{R}$ is the position of the projectile A with respect to that of the target and M is the reduced mass of the system, $M = M_A M_X/(M_A + M_X)$, with $M_A$ and $M_X$ the masses of the projectile and the target, respectively. The Hamiltonian of the isolated target is $H_X(\vec{r}^X)$, with $\vec{r}^X$ denoting the position of the atoms in the target. The operator $\bar{V}$ represents the interaction potential which depends on $\vec{R}$ and on $\vec{r}^X$.

Indicating with $E_\nu$ and $|\nu>$ the internal energy and the internal state of X, respectively, we can write for the unperturbed motion

$$H_0 |\vec{k}\nu> = \left(\frac{\hbar^2 k^2}{2M} + E_\nu\right) |\vec{k}\nu> \quad , \tag{2.4a}$$

$$<\vec{R}\,\vec{r}^X|\,\vec{k}\nu> = (2\pi)^{-3/2}\, e^{i\vec{k}\vec{R}}\, <\vec{r}^X|\nu> \quad , \tag{2.4b}$$

where $\hbar\vec{k}$ is the relative momentum.

Given an interaction potential V between the projectile A and the target X, the collision probability amplitudes may be obtained from the transition operator, T, which satisfies the Lippman Schwinger equation

$$T = V + V\, G_0\, T \quad , \tag{2.5}$$

where $G_0 = (E + i\eta - H_0)^{-1}$ is the propagator for free relative motion of A and X, but involves all the internal motions of X.

Considering scattering from an initial state $|\vec{k}\nu>$, where $\vec{p} = \hbar\vec{k}$ is the relative momentum and $\nu$ is the internal state of the target into a final state $|\vec{k}'\nu'>$, then the scattering rate is given by

$$R(\vec{k}v \rightarrow \vec{k}'v') = (2\pi/\hbar)|\langle \vec{k}'v'|T|\vec{k}v\rangle|^2\delta(E-E') \qquad (2.6)$$

where the $\delta$ function ensures conservation of the total energy of the system. However, since experimental measurements usually correspond to thermal averages over initial distributions, $w_v$, and they only specify $\vec{k}$ and $\vec{k}'$, we must consider the total rate for scattering between initial and final momenta, that is

$$R(\vec{k} \rightarrow \vec{k}') = (2\pi/\hbar)\sum_{v,v'} w_v |\langle \vec{k}'v'|T|\vec{k}v\rangle|^2\,\delta(E-E') \qquad (2.7)$$

The total initial and final energies E and E' must be equal, as it is insured with the $\delta$ function. The sum over final states in Eq (2.7) usually contains a very large number of terms, specially at hyperthermal collision energies. However, by using the completeness of the states and the integral representation of the $\delta$ function

$$\delta(E-E') = \int dt/(2\pi\hbar)\exp[-i(E-E')t/\hbar] \,, \qquad (2.8)$$

the sum over final states may be formally eliminated (Micha, 1986), this gives the result

$$\langle \vec{k}'v'|T|\vec{k}v\rangle\,\delta(E-E') = \int_{-\infty}^{\infty} dt/(2\pi\hbar)\exp(-i\varepsilon t/\hbar)\,\langle \vec{k}'v'| \times \exp(iH_X t/\hbar)\,T\exp(-iH_X t/\hbar)\,|\vec{k}v\rangle \,, \qquad (2.9a)$$

where $H_X$ is the target Hamiltonian, and $\varepsilon$ is the energy transfer defined by,

$$\varepsilon = \hbar^2|k^2 - (k')^2|/2M \,, \qquad (2.9b)$$

The operator T depends on all variables, so its matrix elements

$$T_{\vec{k}',\vec{k}} = \langle \vec{k}'|T|\vec{k}\rangle \,, \qquad (2.10)$$

vary only with the internal variables  Substituting Eq (2 10) into (2 9a) and the latter into Eq (2 7) one arrives at the following expression for the total scattering rate,

$$R(\vec{k},\vec{k}') = \hbar^{-2} \int dt\, e^{-i\omega t/\hbar}\, F_{\vec{k}-\vec{k}'}(t) \ , \tag{2 11a}$$

$$F_{\vec{k}',\vec{k}}(t) = \langle\langle\, T^{\dagger}_{\vec{k}',\vec{k}}(0)\; T_{\vec{k}'-\vec{k}}(t) \,\rangle\rangle \tag{2 11b}$$

$$T_{\vec{k}',\vec{k}}(t) = \exp(i\mathcal{H}_X t/\hbar)\; T_{\vec{k}',\vec{k}}\; \exp(-i\mathcal{H}_X t/\hbar) \ , \tag{2 11c}$$

where the double brackets indicate the quantum mechanical and thermal averages over initial states

The integral in Eq (2 11a) contains the time correlation function (TCF) of the matrix elements $T_{\vec{k}',\vec{k}}$, which are transition operators on internal variables  The time dependence of the transition is given by the internal Hamiltonian of the target  This general equation for the total scattering rate is particularly useful when compared with other approaches which would fail when many internal states are involved  Once the transition operators are expressed in the variables of a given system, the time dependence of the latter may be followed such as one would in a classical treatment

The double differential cross-section for scattering into a unit solid angle $\Omega$ and with a transfer of energy of $\omega$ may be obtained from the ratio of the transition rate to the incident flux (Miche, 1978a), to give

$$d^2\sigma/(d\omega\, d\Omega) = (2\pi/\hbar)^6\, N^2(k'/k) \int_{-\infty}^{\infty} dt\, \exp(\, i\omega t/\hbar)\; x \tag{2 12a}$$

$$\kappa << \hat{T}^{+}_{\vec{k}',\vec{k}}(0)\ \hat{T}_{\vec{k}',\vec{k}}(t) >>/(2\pi\hbar) ,$$

where the relation between the final momentum and the energy transfer is given by

$$k' = (k^2 - 2M\varepsilon/\hbar^2)^{1/2} \qquad (2.12b)$$

The cross-section is thus expressed as the Fourier transform of the time-correlation function of the transition operator.

This correlation function approach allows the development of dynamical approximation to the transition operator in a systematic way, as it is shown in the following section.

## 2.2 The Impulse Approximation

In the regime of hyperthermal collisions, the projectile probes the internal regions of the interaction potential V which is of a multicenter nature. In these cases the potential may be conveniently represented by an expansion about the atomic centers of the target (Micha, 1979a)

$$V(\vec{R},\vec{r}^{\,N}) = \sum_{a} v_a(\vec{R},\vec{r}_a) , \qquad (2.13)$$

The potential $v_a$ represents the interaction between the (A,a) atom pair and depends on the electron distribution of A and on that of the valence state of a in X.

In the formalism of multiple scattering (Rodberg and Thaler, 1967) the many-body transition operator presented in Eq. (2.5) can be expressed in terms of the two body potentials $v_a$, leading to the final channel decomposition

$$T = \sum_{a} T^{(a)}, \qquad (2.14a)$$

$$T^{(a)} = T_a + T_a\, G_0 \sum_{b\neq a} T^{(b)} \,, \tag{2.14b}$$

$$T_a = v_a + v_a\, G_0\, T_a \,, \tag{2.14c}$$

where $T^{(a)}$ corresponds to a final interaction between A and atom a mediated by $v_a$, and $T_a$ is the transition operator when the only allowed interaction is $v_a$, but in which all internal potentials of the target are included in $G_0$.

Introducing the assumption that the majority of collisions involve a single encounter between the projectile atom A and the target atom a, allows us to write $T^{(a)} \approx T_a$. However, in order to calculate $T_a$, a N + 1 body problem must still be solved because $G_0$ involves the motions of all the atoms in the target. This may be substantially simplified whenever the energy transfer occurs in the course of an impulsive collision of the projectile A with atom a.

The basic assumption of the impulse approximation is that a large force $F_a$ acts on an atom a for a period of time $\Delta t$ so short, that all the other forces may be neglected during that time. The position of atom a does not change but its kinetic energy $\langle K_a \rangle_\nu$ in the internal state $\nu$ jumps to a new value $\langle K_a \rangle_{\nu'}$. Energy and momentum are transferred to the target through the interaction between the pair (A,a), while the remaining N-1 atoms in the target provide the restoring forces on a which determine its momentum distribution within the target.

To incorporate these ideas into formulas one can introduce the (A,a) pair-Hamiltonian

$$h_{0,a} = K_R + K_a + E_0 \,, \tag{2.15a}$$

$$K_R = -\hbar^2 \nabla_R^2/(2M) \,, \tag{2.15b}$$

$$K_a = -\hbar^2 \nabla_r^2 / (2m_a) \quad (2.15a)$$

$$E_0 = E_v + \langle K_e \rangle_v = E_{v'} + \langle K_e \rangle_{v'} \quad (2.15b)$$

and the propagator

$$g_{0,a}(E) = (E + i\eta - h_{0,a})^{-1} \quad (2.16)$$

so that the propagator for free relative motion $G_0$ can be written as

$$G_0(E) = g_{0,a}(E) + g_{0,a}(E)\,(K_X - E_0 - K_e)\,G_0(E) \quad (2.17)$$

Substituting Eq (1-17) in the equation for $T_a$, one finds

$$T_a = t_e + t_e (G_0 - g_{0,a})\, T_e \quad (2.18)$$

where

$$t_e(E) = v_e + v_e\, g_{0,a}(E)\, t_a(E) \quad (2.19)$$

Provided $G_0$ and $g_{0,a}$ are close in regions where $t_a$ is different from zero, one can drop the second term in Eq (2.18) and write $T_a = t_a(E)$ which constitutes the impulse approximation

Replacing $T = \sum_a t_a$ in the equation for the total rate, one finds

$$R(\vec{k} \to \vec{k}') = \sum_{a,b} R^{(ba)} \quad , \quad (2.20a)$$

$$R^{(ba)} = \frac{2\pi}{\hbar} \sum_v w_v \sum_{v'} \langle k'v' | t_b | kv \rangle^* \times \langle k'v' | t_a | kv \rangle\, \delta(E - E') \quad , \quad (2.20b)$$

which shows the contribution of each (ab) atom pair in the target. Double differential cross-sections may now be obtained (Micha, 1979b) from the Eqs. (2.20) and one finds

$$\frac{d^2\sigma}{d\varepsilon\, d\vec{\Omega}} = \left(\frac{2\pi}{\hbar}\right)^3 \hbar^2 \left(\frac{k}{k_0}\right) \sum_{a,b} R^{(ba)} \quad (2.21a)$$

$$R^{(ba)} = \frac{2\pi}{\hbar}\,\tau_b(\vec{k}',\vec{k})^*\,\tau_a(\vec{k}',\vec{k})\,S^{(ba)}(\vec{k},\varepsilon)$$

$$S^{(ba)}(\vec{k},\varepsilon) = \sum_{\nu} w_\nu \int \frac{dt}{2\pi\hbar}\, e^{-i\varepsilon t/\hbar}\, \langle \nu | e^{-\frac{i}{\hbar}H_b(\cdots)} e^{\frac{i}{\hbar}\vec{k}\cdot\vec{R}_a(0)} | \nu \rangle$$

(2.21c)

Here $\vec{k}$ is the momentum transfer defined by $\hbar\vec{k} = \hbar(\vec{k}-\vec{k}')$. The factor $\tau_a(\vec{k}',\vec{k})$ involves only the relative motion of the pair (A,a). The second factor, $S^{(ab)}(\vec{k},\varepsilon)$, is the Fourier transform of the atom-pair time-correlation function (Van Hove, 1954) and depends only on the internal dynamics of the isolated target.

The correlation function for a pair of different atoms (a≠b) contains phases that depend on the initial values of the dynamical variables of the target. Experimental conditions usually correspond to initial averages over random phase so that the terms with a≠b average to zero and the cross sections are then given by

$$\frac{d^2\sigma}{d\varepsilon\, d\Omega} = \left(\frac{2\pi}{\hbar}\right)^4 \hbar^2 \frac{k_\varepsilon}{k_0} \sum_a |\tau_a(\vec{k}',\vec{k})|^2\, S^{(aa)}(\vec{k},\varepsilon) \qquad (2.22)$$

Each term in the sum above is a product of a deflection probability and a target absorption probability. The deflection probability can be written as an effective atomic differential cross-section

$$\sigma_a(k',k) = \left(\frac{2\pi}{\hbar}\right)^4 \hbar^2 \frac{k_\varepsilon}{k_0} |\tau_a(\vec{k}',\vec{k})|^2 , \qquad (2.23)$$

in terms of which Eq. (2.22) becomes

$$\frac{d^2\sigma}{d\varepsilon\, d\Omega} = \sum_a \sigma_a(\vec{k}',\vec{k})\, S^{(aa)}(\vec{k},\varepsilon) \qquad (2.24)$$

The impulse approximation presented here will hold provided collisions occur in times short compared with internal motions, and

provided they distort only a local region of the target around a. On the other hand, multiple collision effects may be neglected only for certain conditions on the kinematics and potentials. For example, multiple collision terms would be small for $m_A/m_X << 1$ and $kR_{ab} >> 1$, that is for light projectiles and wavelengths short compared with interatomic distances in the target. Geometric considerations will also play a role when considering multiple collision effects. In general the validity of these assumptions must be reconsidered in each particular case.

## 2.3 Application to Scattering by Adsorbates

Several changes in the structure of a crystal surface can occur when adsorbates are introduced. One of the most important changes is the loss of periodicity which is associated with bare crystal surfaces. In general three cases can be distinguished. In the first case the adsorbates form a regular lattice on the substrate. In such a case the periodicity parallel to the surface is maintained but a new unit cell, usually larger than the original unit cell of the substrate, is needed in order to describe the system. In the second case the periodicity parallel to the surface is destroyed. Here we may think of a single adsorbate on the surface, or a non periodic arrangement of adsorbates. The final case is that in which several layers of atoms are deposited on a metal substrate. In these cases the periodicity of the system as a whole, parallel to the crystal surface, is lost, usually because the adsorbate spacing differs from the atom spacing in the substrate.

The theoretical description of collisions between atoms and adsorbates requires a variety of approaches, depending on the

magnitudes of collision energies on the order and type of surface coverage

The many-body approach has been previously used to study energy transfer in hyperthermal collisions of ions with a solid surface (Niehe, 1981). In such cases the scattering intensity is concentrated around and within surface rainbow angles $\Theta_r$, with single-atom collisions contributing over all scattering angles $\Theta$ while double collisions may contribute at certain angles.

For scattering by light projectiles with energies in the hyperthermal region, where the projectile probes the repulsive region of the adsorbate and of the atoms in the uppermost layer of the substrate, the double differential cross-section is given in a similar way as in the case of surface scattering

$$\frac{d^2\sigma}{d\Omega\, dE} = \sum_i \sigma_1(k,\Theta)\, S^{(11)}(\vec{k},\varepsilon) \,, \qquad (2.25)$$

where i denotes atoms in the target, which can now be adsorbate atoms or surface atoms. Here $\sigma_1(k,\Theta)$ is the elastic differential cross-section for the projectile atom 1 in the target. The surface atoms lie on the plane (x,y,z=0) and the adsorbate is placed at a distance $Z_e$, given by the equilibrium position of the adsorbate above the surface plane. The projectile moves in the direction of decreasing Z, with a certain incident angle $\Theta_i$ measured from the Z axis normal to the surface.

The potential at center i derives from the valence electronic state of atom i in the target and can be obtained from semiempirical potentials whose parameters have been fitted to reproduce experimental data

The elastic differential cr[illegible] $\sigma_i(k,\Omega)$ may then be obtained from a bundle of trajectories with impact parameters b within a bare surface unit cell The factor $S^{(ii)}$ has the meaning of a probability per unit energy for adsorption of momentum $\hbar\vec{K}$ and energy transfer $\varepsilon$.

This self-correlation function, $S^{(ii)}$, must be obtained from a model Hamiltonian for the system A procedure which can be used, appropriate in cases of low coverage, is to describe the target by a finite cluster of N atoms, including the adsorbate and a few layers of the substrate (Parra and Micha, 1976). This model would provide the vibrational modes which are localized in the vicinity of the surface and which are the ones that can be detected by experimental tools

Since scattering from adsorbates resembles scattering from clean surfaces, it is expected that double collisions may contribute at certain scattering angles. The application of Eq. (2.25) is only valid in regions of single collisions However a statistical approach, which uses the geometry of the problem and allows for the description of double collisions, will be presented in a later chapter

CHAPTER 3
VIBRATIONAL FREQUENCIES AND NORMAL MODES
OF MOLECULES ADSORBED ON SURFACES

The vibrational spectra of molecules adsorbed on metal surfaces can be studied with a variety of experimental techniques involving scattering of electrons (Ibach and Mills, 1982), photons, neutrons and neutral or ionized atoms (Willis, 1980). The spacings and shapes of spectral lines provide information about the conformation of the adsorbate and its substrate, and about the force field that determines the vibration dynamics.

When the probing particles are atoms, translational energy is transferred into both adsorbate and substrate, possibly resulting in the shift and reshaping of spectral lines. The theoretical interpretation of the spectra can be simplified when the internal dynamics of the adsorbate can be identified and separated from the collision dynamics.

The normal modes of adsorbates on solid surfaces can be obtained from generalizations of theories developed for surface lattice dynamics. Approaches can be based on Green functions (Rahman, Black and Mills, 1982), slab models with a small number of layers (Strong et al., 1982), and cluster models. Green functions require extensive work while cluster calculations, although less involved, may not always properly describe the influence of site symmetry (Rahman et al., 1983). Furthermore, they have been used together with simple force fields of the central-field type. However, one expects that more detailed force fields will be needed, containing in particular

bending forces, when one wishes to describe the collisional excitation of adsorbate vibrations.

Cluster models have been found adequate to describe adatoms (Bleck et al., 1982), and in some cases have been as effective as models based on periodic small clusters (Bleck, 1982). Applied to molecular adsorbates, these models can be parametrized to incorporate what is known about the vibrational modes of the isolated molecule and clean surface. They also allow for detailed valence-force fields and for the interpretation of the point group symmetry of the adsorption site.

Experimental studies (Andersson, 1977) of CO on Ni(001) have provided evidence that CO molecules can bind on a top site above a Ni atom, on a bridge site between two of them or in a mixture of both (Bertolini and Tardy, 1981). For a dilute CO lattice gas on Ni(001), two peaks are observed, at 239 and 256 meV, in electron energy loss spectra (EELS). However, at higher coverages only a single peak at 256 meV is observed. These findings have been interpreted as due to the presence of both top and bridge species in the case of low coverages, but of only the on-top species in the higher coverages (Andersson and Pendry, 1979).

Model calculations on small clusters have been performed by several workers to obtain vibrational frequencies of a CO molecule adsorbed on a nickel surface. The frequencies of a $Ni_5CO$ cluster for the on-top site and a $Ni_6CO$ cluster for the bridge site have been analyzed (Richardson and Bradshaw, 1979), in terms of semi empirical force fields, with only the C and O atoms moving. The frequencies of a linear $Ni_2CO$ molecule have been calculated using ab initio methods

(Allison and Goddard, 1982) based on general equations for XYZ type molecules.

In this chapter, we develop a simple cluster model of diatomic adsorption and apply it to CO adsorbed on Ni(001). It is based on a more detailed, valence-force field than previously found in the literature, and it incorporates site symmetry. It also allows for moving surface atoms so that a more detailed picture of the adsorbate dynamics can be derived. Furthermore, the substrate cluster contains two surface modes whose frequencies can be fitted to known values at the Γ-point of the surface Brillouin zone.

We analyze the frequencies of a CO molecule adsorbed on Ni(001) using two different clusters, intended to model the on-top and bridge species. Section 3.1 describes the conformation and force fields for the clusters. Section 3.2 presents the normal mode analysis based on the FG method of molecular spectroscopy (Wilson, Decius and Cross, 1955). The numerical results and figures showing the normal modes are given in section 3.3.

## 3.1 Cluster Models and Force Fields

To model adsorption at the on top site, we use an eleven-atom cluster, shown in Fig. 3.1, containing C, O and nine Ni atoms, with C, O and one Ni atom allowed to move. This cluster contains all metal atoms that are nearest neighbors to the bonding site: four in the first layer and four in the second layer, with the CO bonded to a Ni atom in the face centered cubic structure.

In the bridge-bonded situation, we have chosen a 16-atom cluster, shown in Fig. 3.2, that contains fourteen Ni atoms, of which the two bonded to C are allowed to move. This cluster also contains all

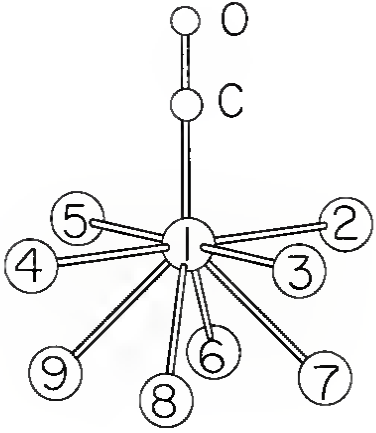


Figure 3.1 On-Top Cluster: Nickel atoms with numbers 1 to 5 correspond to surface atoms, and with numbers 6 to 9 to nearest neighbors in the second layer; C O and nickel atom 1 are the only ones allowed to move.

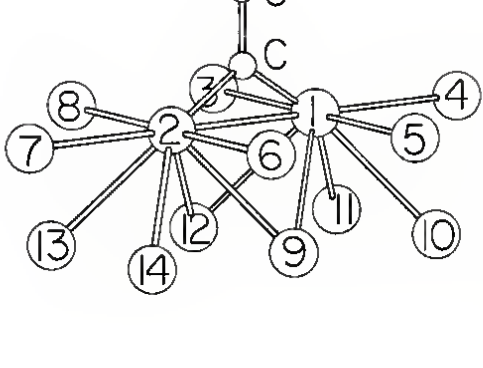


Figure 3-2. Bridge Cluster. Nickel atoms with numbers 1 to 8 correspond to surface atoms, and with numbers 9 to 14 to nearest neighbors in the second layer, C,O and nickel atoms 1 and 2 are the only ones allowed to move. The height of the C atom above the surface ($d_C$) is determined by the angle Ni C Ni

metal atoms that are nearest neighbors to the two metal atoms representing the bonding site, six in the first layer and six in the second layer. The carbon atom of the CO molecule is bonded to two nickel atoms, one in a position corresponding to a face center atom and the other one corner in the face centered cubic structure.

A $C_{4v}$ point group can be associated to the top bonding situation whereas a $C_{2v}$ point group is more appropriate for the bridge model. Since on a real surface all translation and rotations are restricted, we expect all 3N degrees of freedom to be vibrational modes. Therefore, we should find 3 x 3 = 9 vibrational modes for the top case. These can be classified as three hindered translations, two hindered rotations and four modes which are equivalent to the vibrational modes of an XYZ isolated linear molecule in the gas phase.

The latter could also be considered as arising from the vibration of the isolated CO molecule interacting with two phonon modes of the substrate represented by a single nickel atom.

For the bridge bonded situation two of the metal atoms are allowed to move, given a total of 3 x 4 = 12 vibrational modes; six of these correspond to the molecular modes of a $X_2CO$ isolated molecule in the gas phase. Again this could also be considered as the vibration of the CO molecule interacting with four phonon modes of the substrate represented by two nickel atoms.

In order to carry out calculations of the frequencies, to obtain the actual form of the normal modes and to classify the different vibrational modes according to the symmetry of the clusters, we have chosen a valence force field to represent the potential energy of the clusters.

Usually, the potential energy is expressed in terms of the changes in the internuclear distances and in a number of angles. For the on-top position we used a total of 12 internal coordinates, eight of these coordinates to represent the changes in the Ni-Ni internuclear distances, one each for the changes in CO and NiC bond distances, one for the change in the angle between the CO and C Ni bond and one for the change in the angle between C-Ni bond and the adjacent Ni-Ni bond.

Denoting by $s_{ij}$ the changes in the Ni-Ni internuclear distances, by $s_{CO}$ and $s_{CNi}$ the changes in CO and CNi bond distances and by $s_\theta$ and $s_\gamma$ the changes in the angles described above, the potential energy $V^T$ for the on-top cluster is given by

$$2V^T(s) = f_{Ni}^{(1)} \sum_{j=2}^{5} s_{1j}^2 + f_{Ni}^{(2)} \sum_{k=6}^{9} s_{1k}^2 + f_{CNi}\, s_{CNi}^2 + f_{CO}\, s_{CO}^2 + f_\theta\, s_\theta^2 + f_\gamma\, s_\gamma^2 \qquad (3.1)$$

In the above expression the subscript 1 had been used to denote the metal atom bonded to the CO molecule, $f_{Ni}^{(1)}$ and $f_{Ni}^{(2)}$ denote the force constants for the interaction between neighboring atoms in the first layer and that between first and second layer atoms.

A total of 22 coordinates were used for the bridge bonded model; 15 to represent changes in the Ni Ni internuclear distances, 3 to represent changes in the bond distances of the adsorbed molecule and four to represent changes in the angles.

Denoting by $s_\delta$ the change in the angle between the CNi bonds, by $s_\varepsilon$ the change in the angle between the CO bond and the plane Ni-C-Ni, and by $s_\theta$ and $s_\gamma$ the same variables as for the on-top position, the potential energy $V^B$ can be written as

$$2V^{B}(s) = f_{Ni}^{(1)} \left( \sum_{j=2}^{5} e_{1j}^2 + \sum_{j=6}^{8} s_{2j}^2 \right) + f_{Ni}^{(2)} \left| \sum_{k=9}^{12} s_{1k}^2 + \sum_{k=9,12}^{14} s_{2k}^2 \right| \quad (3.2)$$

$$+ f_{CO}\, s_{CO}^2 + f_{CNi}\, s_{CNi}^2 + f_a\, s_a^2 + f_d\, s_d^2 + f_g\, s_g^2 + f_b\, s_b^2 .$$

Phonon dispersion curves have been obtained (Black et al., 1981) for the Ni(001) surface at different points of the substrate Brillouin zone. Two surface modes with frequencies of 104.7 and 125.5 $cm^{-1}$ and polarizations parallel to the surface and normal to the surface, respectively, were found at the $\Gamma$ zone boundary point. These values were used to fit the two force constants $f_{Ni}^{(1)}$ and $f_{Ni}^{(2)}$ in Eq. (3.2). The intermolecular distances and the other force constants were taken from data for $Ni(CO)_4$, (Jones, 1960). For the bridging species the force constants $f_d$ and $f_g$ were fitted to reproduce the frequencies for a molecule of the type $X_2CO$ (Herzberg, 1945), which is the limiting case of the bridge cluster after the neighboring atoms of the Ni bonded to the CO molecule have been taken away. The chosen force constants and geometric parameters are presented in Table 3.1 and 3.2 respectively, where $d_{Ni}$ is the distance between nearest neighbors in the bulk crystal structure, and $d_C$ is the distance from the C atom to the surface in Fig. 3.2. As a preliminary check of the model and the chosen field, we calculated the frequencies of an isolated XYZ molecule to represent the limiting case for the on top position cluster. The results are within 1 $cm^{-1}$, as can be seen in Table 3.3, from those obtained by an ab initio calculation on the same molecule (Allison and Goddard, 1982).

For the cluster representing the bridge bonded situation, the limiting case was $H_2CO$, obtained by replacing in our cluster the

Table 3.1 [illegible] Internal Coordinate Sets

| Force Constants | Tmp | Bridge |
|---|---|---|
| $f_{CO}$ (mdyne $Å^{-1}$) | 17.0 | 14.7 |
| $f_{CNi}$ (mdyne $Å^{-1}$) | 2.1 | 1.9 |
| $f_{Ni}^{(1)}$ (mdyne $Å^{-1}$) | 0.15 | 0.15 |
| $f_{Ni}^{(2)}$ (mdyne $Å^{-1}$) | 0.27 | 0.27 |
| $f_a$ (mdyne Å $rad^{-2}$) | 0.38 | 0.38 |
| $f_b$ (mdyne Å $rad^{-2}$) | 0.23 | 0.23 |
| $f_d$ (mdyne Å $rad^{-2}$) | | 0.23 |
| $f_g$ (mdyne Å $rad^{-2}$) | | 0.38 |

Table 3.2 Geometric Parameters of Clusters

| Geometric Parameters | Tmp | Bridge |
|---|---|---|
| $d_{CO}$ (Å) | 1.15 | 1.15 |
| $d_{CNi}$ (Å) | 1.84 | 1.80 |
| $d_{Ni}$ (Å) | 2.49 | 2.49 |
| $d_C$ (Å) | | 0.84 |
| Ni-C-Ni angle (deg) | | 112.00 |

Table 3.3 Comparison of Vibrational Fr[illegible] for a Linear HiCO Molecule

| Normal Mode | Our Results | (Allison and Goddard, 1982) |
|---|---|---|
| CO Stretch | 2130.5 | 2129 |
| NiC Stretch | 400.6 | 401 |
| NiCO Bend | 327.8 | 327 |

masses and force constants of the two nickel atoms bonded to CO by hydrogen masses and force constants, and setting to zero all other unnecessary force constants. The calculated frequencies were found to be within less than 100 $cm^{-1}$ when compared to experimental results for formaldehyde (Clouthier and Ramsay, 1983).

## 3.2 Normal Mode Analyses

Expressions (3.1) and (3.2) in Section 3.1, for the potential energy of the clusters, contain far more coordinates than the degrees of freedom of the clusters.

In order to reduce the number of coordinates to equal the number of degrees of freedom of the clusters we recall that only a reduced number of atoms are allowed to move, this relates the internal coordinates $\{s\}$ to the atomic cartesian displacements (x,y z). After expanding around the equilibrium position and setting to zero the displacements of the atoms other than Ni, C and O, we obtain the transformation

$$\underset{\sim}{s} = \underset{\sim}{A}\,\underset{\sim}{X} \qquad (3.3)$$

Here $\underset{\sim}{X}$ is a column vector with the cartesian displacements of the three moving atoms. Using the point group symmetry of the clusters,

a set of symmetry coordinates (S) was constructed from the atomic displacements X. The transformation

$$\underline{S} = \underline{U}\ \underline{X}\ , \qquad (3\text{-}4)$$

allowed us to determine a new force constant matrix which is block diagonal according to the symmetry of each cluster. The successive transformation are represented by

$$2V(S) = \underline{S}^t\ \underline{f}\ \underline{S} \xrightarrow{A} \underline{X}^t\ \underline{k}\ \underline{X} \xrightarrow{U} \underline{S}^t\ \underline{F}\ \underline{S} \qquad (3\ 5)$$

The relations between the different coordinates are listed in the Appendices A and B. The final F matrices are presented in Table 3 4 for the on-top cluster and Table 3-5 for the bridge.

Frequencies were calculated using F and G matrix method (Wilson, Decius and Cross, 1955). The G matrix is defined by the kinetic energy T. Starting with

$$2T = (\dot{\underline{X}})^t\ \underline{M}\ \dot{\underline{X}}\ , \qquad (3\ 6)$$

and, using $\underline{S} = \underline{U}\ \underline{X}$, one can then write

$$2T = (\dot{\underline{S}})^t\ \underline{G}^{-1}\ \dot{\underline{S}}\ , \qquad (3\ 7)$$

where $\underline{G}^{-1} = (\underline{U}^{-1})^t\ \underline{M}\ \underline{U}^{-1}$ and M is the diagonal matrix of masses. From these F and G matrices, one obtains the frequencies corresponding to the normal modes by solving

$$(\underline{GF})\ A_k = \lambda_k\ A_k\ , \qquad (3\text{-}8)$$

where, introducing the speed of light c, frequencies $\nu_k$ are given by

$$\lambda_k = (2\pi c \nu_k)^2\ , \qquad (3\ 9)$$

and the corresponding normal modes by

$$\underline{Q} = \underline{A}^{-1}\ \underline{S} \quad \text{or} \quad \underline{Q} = (\underline{A}^{-1}\ \underline{U})\ \underline{X} \qquad (3\ 10)$$

Table 3.4 F Matrix for On-top Cluster

$F_{11} = 2 f_{Ni}^{(2)} + f_{CNi}$ $F_{12} = - f_{CNi}$

$F_{22} = f_{CNi} + f_{CO}$ $F_{23} = - f_{CO}$

$F_{44} = 2f_{Ni}^{(1)} + f_{Ni}^{(2)} + (f_a + f_b)/d_{CNi}^2$ $F_{33} = f_{CO}$

$F_{46} = f_a(d_{CNi} + d_{CO})/(d_{CO}d_{CNi}^2) - f_b/d_{CNi}^2$ $F_{55} = F_{44}$

$F_{48} = f_a/(d_{CO}d_{CNi})$ $F_{57} = F_{46}$

$F_{66} = f_a[(d_{CNi} + d_{CO})/(d_{CNi}d_{CO})]^2 + f_b/(d_{CNi})^2$ $F_{59} = F_{48}$

$F_{68} = -f_a (d_{CNi} + d_{CO})/(d_{CNi}d_{CO}^2)$ $F_{77} = F_{66}$

$F_{88} = f_a/(d_{CO})^2$ $F_{99} = F_{88}$

Table 3.5 F Matrix for Bridge Cluster

$A_1$ Symmetry

$F_{11} = 2(a_3 - a_4)^2 f_a + 2(d_C/d_{CNi})^2 f_{CNi} + f_{CO} + 4b_1^2 f_g$

$F_{12} = 2a_4(a_3 - a_4) f_a - f_{CO}$

$F_{13} = -(2/\sqrt{2}) a_3(a_3 - a_4) f_a - (2/\sqrt{2})(d_C/d_{CNi})^2 f_{CNi} - (4\sqrt{2}) b_1^2 f_b$

$F_{14} = -(2/\sqrt{2}) b_1 d_C f_{CNi} - (2/\sqrt{2}) a_2 (a_3 - a_4) f_a + (4/\sqrt{2}) b_2 a_2 f_g$

$F_{22} = 2a_4^2 f_a + f_{CO}$

$F_{23} = -(2/\sqrt{2}) a_3 a_4 f_a$

TABLE 4.3 (continued)

$F_{23} = (2/\sqrt{2})\, a_2 a_4 f_a$

$F_{33} = a_3^2 f_a + (d_C/d_{CN1})^2 f_{CN1} + (1/(d_{CN1}d_{N1})^2 f_b + a_4^2 f_z$
$+ (40/21) f_{N1}^{(2)}$

$F_{34} = a_2 a_3 f_a - (d_C/d_{N1})(1/d_{CN1})^2 f_b \quad (d_C d_{N1}/2d_{CN1}^2) f_{CN1}$
$- 2b_1 a_2 f_z - (4/7)(1/\sqrt{2})\, f_{N1}^{(2)}$

$F_{44} = a_2^2 f_a + (d_{N1}/d_C)^2 F_{CN1} + 2a_2^2 f_z + (1/2d_{CN1}^2) f_b$
$+ (17/5) f_{N1}^{(1)} + (8/7) f_{N1}^{(2)}$

where,

$a_1 = 1/d_{CO} \qquad a_2 = d_C/d_{CO}^2 \qquad a_3 = -2(d_C^2 + d_{CN1}^2)/(d_{N1}d_{CN1}^2)$

$a_4 = -4\, d_C/(d_{N1}d_{CO}) \qquad b_1 = -d_{N1}/(2\, d_{CN1}^2)$

---

$B_2$ Symmetry

---

$F_{11} = a_3^2 f_a + (d_C/d_{CN1})^2 f_{CN1} + (40/21) f_{N1}^{(2)} + 2(d_C/d_{N1}d_{CN1})^2 f_b$

$F_{12} = (2/\sqrt{2})\, a_3(a_2 - a_1) f_a \quad (1/\sqrt{2})(d_{N1}d_C/d_{CN1}^2) f_{CN1}$

$F_{13} = (2/\sqrt{2})\, a_1 a_3 f_a$

$F_{14} = (d_{N1}d_C/2d_{CN1}^2) f_{CN1} + (4\sqrt{2}/7) f_{N1}^{(2)} - a_2 a_3 f_a + (d_C/2d_{N1}d_{CN1}^2) f_b$

$F_{22} = (1/\sqrt{2})(d_{N1}/d_C)^2 f_{CN1} + 2(a_2 - a_1)^2 f_a$

$F_{23} = 2a_1(a_2 - a_1) f_a$

$F_{33} = 2a_1^2 f_a$

Table 3 5 (continued)

$$F_{24} = -(2/\sqrt{2})\,\sigma_2(\sigma_2 - \sigma_1)\,f_a - (1/2\sqrt{2})\,(d_{N1}/d_{CN1})^2\,f_{CN1}$$

$$F_{34} = (2/\sqrt{2})\,\sigma_1\sigma_2 f_a$$

$$F_{44} = \sigma_2^2 f_a + (d_{N1}/2d_{CN1})^2\,f_{CN1} + f_b/(2d_{CN1}^2)\,f_b + (7/5)\,f_{N1}^{(1)} + (6/7)\,f_{N1}^{(2)}$$

---

$A_2$ Symmetry

$$F_{11} = (8/5)\,f_{N1}^{(1)} + (20/21)\,f_{N1}^{(2)} + (2/d_{CN1}^2)\,f_b$$

---

$E_1$ Symmetry

$$F_{11} = (4/d_{CN1}^2)\,f_b + [(d_C + d_{CO})/(d_C\,d_{CO})]^2\,f_d$$

$$F_{12} = -f_d\,(d_C + d_{CO})/(d_C\,d_{CO}^2)$$

$$F_{13} = -4f_b/(\sqrt{2}\,d_{CN1}^2) - f_d(d_C + d_{CO})/(\sqrt{2}\,d_{CO}d_C^2)$$

$$F_{22} = f_d/d_{CO}^2 \qquad F_{23} = f_d/(\sqrt{2}\,d_C d_{CO})$$

$$F_{33} = (8/5)\,f_{N1}^{(1)} + (20/21)\,f_{N1}^{(2)} + f_d/(2d_C^2) + 2f_b/d_{CN1}^2$$

The matrices $\underline{GF}$ constructed in this way reflect the symmetries of the clusters, thus simplifying the calculation and the classification of the modes according to the symmetry of the clusters In the on-top case the resulting GF matrix is block diagonalized into one 3 x 3 matrix belonging to the $A_1$ irreducible representation, and one 6 x 6 matrix containing two coupled modes belonging to the E irreducible

representation The GF matrix in the bridge case is 12 x 12 but block-diagonalizes into two 4 x 4 matrices, one belonging to the $A_1$ and the other to the $B_2$ irreducible representations, one 3 x 3 matrix belonging to the $B_1$ and one 1 x 1 matrix belonging to the $A_2$ irreducible representation.

### 3.3 Numerical Results for CO on Ni(001)

The vibrational modes for the on top and bridge clusters are shown in Figures 3.3 and 3.4, respectively. The resulting coefficients for the transformation from cartesian to normal coordinates are presented for the on-top and bridge clusters, in Appendix C. We separately discuss the on top and bridge cases.

#### 3.3.1 The On Top Cluster

The calculated frequencies along with previous experimental and theoretical results are presented in Table 3.6 for the on-top cluster. In this case we find one frequency $\nu_1^A$ with value comparable to the CO stretching for the free molecule, 2143.2 $cm^{-1}$, and two frequencies $\nu_2^A$ and $\nu_4^E$ with values similar to the experimental frequencies (of 381 $cm^{-1}$ for CNi stretch, and of 461 $cm^{-1}$ for NiCO bend) found in carbonyl compounds, $Ni(CO)_4$ (Crawford and Horwitz, 1948). We also find three frequencies $\nu_3$, $\nu_5$ and $\nu_6$ with values lower than the largest frequency for the bare substrate phonon band, 295 $cm^{-1}$ (Black et al., 1981).

The mode with the highest frequency, $\nu_1$, is related to the free molecule CO stretch, $\nu_2$ relates to the Ni C stretching mode, and the $\nu_3$ mode can be considered as a frustrated translation along the direction normal to the surface.

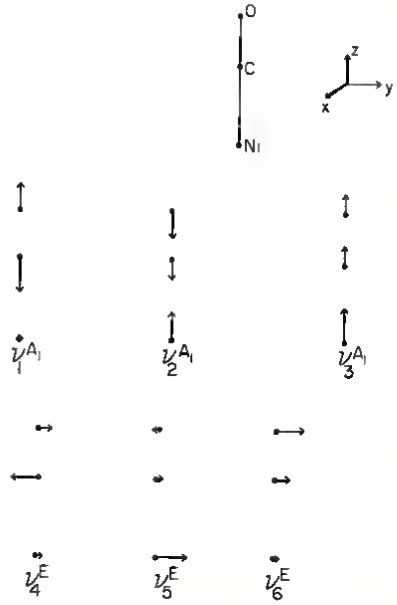


Figure 3 3: Normal Vibrational Displacements for the On Top Cluster. The ν-symbol label different irreducible representations for each symmetry group.

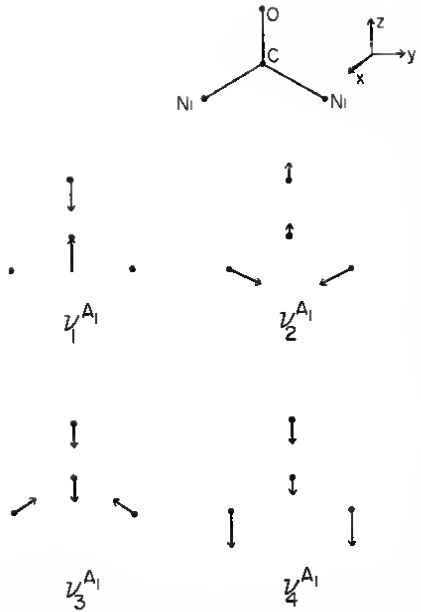


Figure 3 4: Normal Vibrational Displacements for the Bridge Cluster.

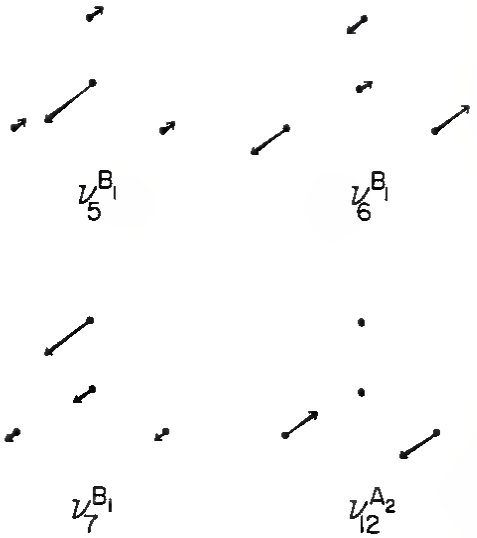


Figure 3-4 continued

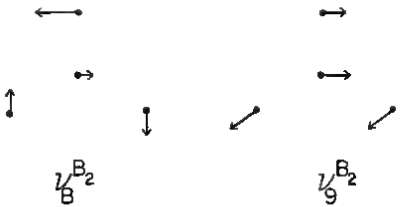


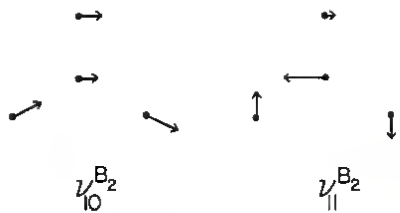


Figure 3.4 continued

Table 3 6 Comparison of Results, On-Top Cluster (Frequencies in $cm^{-1}$)

| | $\nu_1^{A_1}$ | $\nu_2^{A_1}$ | $\nu_3^{A_1}$ | $\nu_4^{E}$ | $\nu_5^{E}$ | $\nu_6^{E}$ |
|---|---|---|---|---|---|---|
| Experiment (Andersson 1977) | 2069 | 480 | | | | |
| Our Results | 2083 | 431 | 102 | 389 | 131 | [illegible] |
| NiCO (Richardson and Bradshaw, 1979) | 2083 | 437 | | 411 | 82 | |
| $Ni_3CO$ (Black et al., 1982) | 2088.3 | 431.7 | 98.6 | 399.2 | 142.1 | 71.6 |
| $Ni_2CO$ Periodic Cluster (Black, 1982) | 2087.5 | 430.6 | 84.7 | 399.6 | 208 | 67.3 |
| Spectral Density (Black et al. 1982) | 2083.3 | 440.3 | 148 | 400.6 | 190 | 37 |

Three modes which belong to the E representation, $\nu_4$, $\nu_5$ and $\nu_6$, can be considered as two frustrated rotations ($\nu_4$ and $\nu_5$), about the x and y axes, and a frustrated translation ($\nu_6$) along a direction parallel to the surface. These assignments are shown in Table 3.7.

The values obtained for the C-O stretch and Ni-C stretch are in fairly good agreement with the values assigned to the on-top bonded CO (Andersson, 1977). For the three higher frequencies we obtain results almost identical to the ones for a $(Ni)_5CO$ cluster and also to the ones for a periodic lattice of small clusters, $(Ni)_2CO$ (Black, 1982); the latter used only nearest neighbor interactions and a central force field.

We obtain two frequencies at 389 and 44 $cm^{-1}$, with values higher and lower than the largest bare substrate phonon frequency that are

Table 3.7 Designation, Character, Species and Frequencies of the Normal Modes for On Top Cluster

| Description | $A_1$ | E | Frequency ($cm^{-1}$) |
|---|---|---|---|
| C-O Stretching | $\nu_1$ | | 2088 |
| C-Ni Stretching | $\nu_2$ | | 431 |
| Ni-C-O Frustrated Translation (Perpendicular to Surface) | $\nu_3$ | | 102 |
| O-C-Ni Bending | | $\nu_4$ | 389 |
| Ni-C-O Frustrated Rotation | | $\nu_5$ | 131 |
| Ni-C-O Frustrated Translation (Parallel to Surface) | | $\nu_6$ | 44 |

in very good agreement with two frustum like modes at 37 and 400 cm$^{-1}$ obtained in calculations of the spectral density function of a periodic $(Ni)_2CO$ cluster using green function methods (Bleck, 1982).

We also obtained a value of 102 cm$^{-1}$ for the mode which involves motion perpendicular to the surface ($\nu_3^{A_1}$); this value, although higher than the one obtained by Black for the overlayer and for the isolated $(Ni)_5CO$ cluster, could be associated to the fairly broad peak centered at 148 cm$^{-1}$ obtained in the spectral density calculations for the full crystal.

3.3.2 The Bridge Cluster

For the bridge model we found a total of 12 modes, four with $A_1$ symmetry, three with $B_1$ symmetry, four with $B_2$ symmetry and one with $A_2$ symmetry. The frequencies $\nu_1^{A_1}$, $\nu_2^{A_1}$, $\nu_3^{A_1}$, $\nu_5^{B_2}$, $\nu_8^{B_2}$, and $\nu_9^{B_2}$, have values similar to molecular mode frequencies, and the remaining $\nu_4^{A_1}$, $\nu_6^{B_1}$, $\nu_7^{B_1}$, $\nu_{10}^{B_2}$, $\nu_{11}^{B_2}$ and $\nu_{12}^{A_2}$ have values lower than the largest bare substrate phonon frequency (295 cm$^{-1}$). These calculated frequencies are presented in Table 3.8 along with results from other calculations and previous experimental results.

The $A_1$ mode with the largest frequency, $\nu_1$, can be easily recognized as a CO stretch, $\nu_2$ is a NiC symmetric stretch and the other two, $\nu_3$ and $\nu_4$, can be considered as frustrated transitions in a plane normal to the surface, with the last two modes involving C-Ni Ni bending. Three bending modes belonging to the $B_1$ representation involve motions out of the plane formed by the two nickel atoms and the carbon, one of these, $\nu_5$, can be considered as a frustrated translation and the other two, $\nu_6$ and $\nu_7$, as $OC(Ni)_2$ bendings. A summary of these assignments is shown in Table 3.9

Table 3 8 Comparison of Results, Bridge Cluster
(Frequencies in $cm^{-1}$)

| Frequency | Experiment (Andersson, 1977) | Our Results | (Richardson & Bradshaw, 1979) |
|---|---|---|---|
| $\nu_1^{A_1}$ | 1932 | 1981 | 2099 |
| $\nu_2^{A_1}$ | | 530 | |
| $\nu_3^{A_1}$ | 359 | 366 | 457 |
| $\nu_4^{A_1}$ | | 53 | |
| $\nu_5^{B_1}$ | | 569 | 572 |
| $\nu_6^{B_1}$ | | 125 | |
| $\nu_7^{B_1}$ | | 71 | 76 |
| $\nu_8^{B_2}$ | 657 | 764 | 649 |
| $\nu_9^{B_2}$ | | 397 | 184 |
| $\nu_{10}^{B_2}$ | | 68 | |
| $\nu_{11}^{B_2}$ | | 2 | |
| $\nu_{12}^{A_2}$ | | 143 | |

Table 3.9 Designation, Character, Species and Frequencies of the Normal Modes for Bridge Cluster

| Description | $A_1$ | $E_1$ | $E_2$ | $A_2$ | Frequencies ($cm^{-1}$) |
|---|---|---|---|---|---|
| C-O Stretching | $\nu_1$ | | | | 1981 |
| C-Ni Symmetric Stretching | $\nu_2$ | | | | 530 |
| C-Ni Asymmetric Stretching | $\nu_3$ | | | | 366 |
| Frustrated Translation (z axes) | $\nu_4$ | | | | 53 |
| $OC(Ni)_2$ Bending | | $\nu_5$ | | | 569 |
| Frustrated Rotation (y axes) | | $\nu_6$ | | | 125 |
| Frustrated Translation (x axes) | | $\nu_7$ | | | 71 |
| Antisymmetric NiC Stretching | | | $\nu_8$ | | 764 |
| Frustrated Rotation (x axes) | | | $\nu_9$ | | 397 |
| Frustrated Translation (y axes) | | | $\nu_{10}$ | | 68 |
| Combination of 8 and 9 | | | $\nu_{11}$ | | 2 |
| Frustrated Rotation (z axes) | | | | $\nu_{12}$ | 143 |

The present procedure includes several metal atoms to represent the metal substrate and at the same time restricts the number of degree of freedom of the cluster to describe the vibrational modes of a molecule attached to metal atoms at a surface. The calculations yield vibrational frequencies which are in good agreement with experimental results available on the system. Some of the

frequencies presented here describe new modes for the bridge cluster which have not been presented in previous works

A fairly clear distinction, see energy diagram shown in Figure 3.5, can be made between modes with relative high frequencies (molecular modes) and those which correspond to soft modes coming from the interaction of the adsorbate with the modes of the bare substrate. This separation of modes is more evident for the bridge case than for the top case

These cluster models and their frequencies and normal modes can be used as a first step in the study of atoms scattered by adsorbates.

Figure 3.5 Comparison on Energies for the isolated CO Molecule, the Bare Nickel Substrate and the Results Obtained for the On-Top and Bridge Cluster

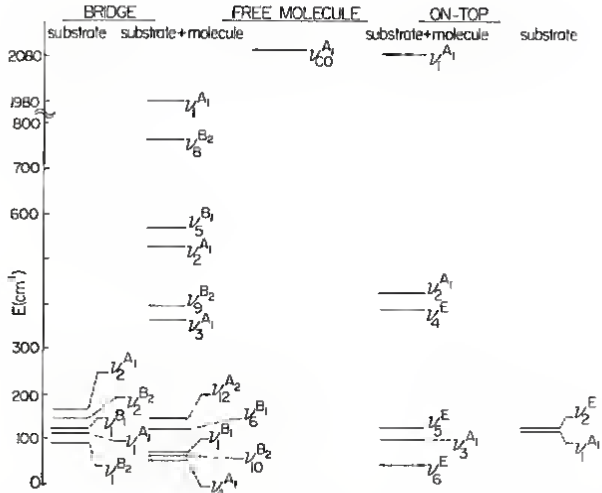
BRIDGE
substrate
substrate+molecule
FREE MOLECULE
ON-TOP
substrate+molecule
substrate
E(cm⁻¹)
2080
1980
800
700
600
300
200
100
0
$\nu_{CO}^{A_1}$
$\nu_1^{A_1}$
$\nu_1^{A_1}$
$\nu_8^{B_2}$
$\nu_5^{B_1}$
$\nu_2^{A_1}$
$\nu_9^{B_2}$
$\nu_3^{A_1}$
$\nu_2^{A_1}$
$\nu_4^{E}$
$\nu_2^{A_1}$
$\nu_2^{B_2}$
$\nu_1^{B_1}$
$\nu_1^{A_1}$
$\nu_1^{B_2}$
$\nu_{12}^{A_2}$
$\nu_6^{B_1}$
$\nu_1^{B_1}$
$\nu_{10}^{B_2}$
$\nu_{11}^{A_1}$
$\nu_5^{E}$
$\nu_3^{A_1}$
$\nu_6^{E}$
$\nu_2^{E}$
$\nu_1^{A_1}$

# CHAPTER 4

## ENERGY TRANSFER INTO MOLECULAR ADSORBATES

In scattering by adsorbates leading to energy transfer, the translational degrees of freedom can frequently be described classically while the remaining ones, only vibrational degrees of freedom in our case, must be treated as quantized.

It was pointed out in Chapter 2, that by relating inelastic scattering cross sections to time-correlation functions (TCF's) of transition amplitudes, it is possible to study energy transfer in scattering by extended targets without having to expand wavefunctions in the many excited states of the target. Inelastic scattering cross-sections for collisions in which the relative momentum changes from $\hbar\vec{k}_i$ to $\hbar\vec{k}_f$ were shown to be given by the Fourier transform of the TCFs of the operators $\langle\vec{k}_f|T|\vec{k}_i\rangle$, where T is the transition operator of scattering theory.

For experimental conditions of high relative energy and light projectiles, the interaction is dominated by strong short range repulsive forces, and lasts a short time compared with the periods of internal motions of the target, so that an impulsive model is appropriate. Under these conditions, as was shown in Chapter 2, the double differential cross-section is obtained from TCFs involving the position operators of the target atoms. We show in Sec. 4-1 how to obtain the vibrational TCFs analytically from the normal vibrational modes of the target. Furthermore, since the normal modes of the

target can be grouped in two sets, slow and fast modes, we can approximate the TCFs by short-time expansions which lead to Gaussian distributions of the energy transferred into the slow modes, as shown in Sec. 4.2. Finally, in Sec. 4.3, we introduce a statistical model which allows us to obtain a simple description of double collisions.

### 4.1 The Vibrational Correlation Function

The TCF of position of the target atoms that we wish to calculate is given by

$$P^{(aa)}(\vec{R},t) = \langle\langle \exp[-i\vec{R}\,\vec{r}_a(0)] \exp[i\vec{R}\,\vec{r}_a(t)] \rangle\rangle , \qquad (4.1a)$$

with

$$\langle\langle \ldots \rangle\rangle = \sum_v w_v \langle v|\ldots|v\rangle , \qquad (4.1b)$$

which includes the quantum-statistical average over the distribution $w_v$ of initial vibrational states $|v\rangle$ of the target. Indicating operators with carets, $\hat{r}_a(t)$ corresponds to the instantaneous position of atom a, which evolves in time in accordance with the Hamiltonian $\hat{H}_X$ of the isolated target as follows:

$$\hat{r}_a(t) = \exp(i\hat{H}_X t/\hbar)\, \hat{r}_a \exp(-i\hat{H}_X t/\hbar) \qquad (4.2)$$

For each atom a in the target we can introduce its equilibrium position $\vec{d}_a$ and displacement from equilibrium $\vec{u}_a$, so that

$$\vec{r}_a = \vec{d}_a + \vec{u}_a . \qquad (4.3)$$

In a body-fixed reference frame we have $N_v = 3N$ free vibrational coordinates, where N is the number of atoms in the target. Using Eq. (4.3) in Eq. (4.1a) we obtain

$$F^{(coh)}(\vec{K},t) = << \exp\{-iK\,[\vec{d}_a(0) + \vec{u}_e(0)]\}$$

$$\times \exp\{iK\,[\vec{d}_a(t) + \vec{u}_e(t)]\} >>_v \qquad (4.4)$$

The target Hamiltonian is nothing but $H_v$ and from $[H_v, \vec{d}_a] = 0$, we find that

$$F_{vK}(t) = << \exp[-i\vec{K}\,\vec{u}_e(0)]\,\exp[iK\,\vec{u}_e(t)] >>_v \qquad (4.5)$$

Assuming harmonic vibrations as a zeroth order approximation, which is acceptable except for highly excited vibrational levels near the dissociation energy, and using internal coordinates $s_i$ which are linearly related to the displacements by

$$\vec{u}_e = \sum_{i=1}^{n_v} \vec{A}_{ei}\, s_i \ , \qquad (4.6)$$

the vibrational TCF is most conveniently evaluated in terms of the normal displacements $Q_j(t) = Q_j(0)\cos\omega_j t$, which are related to the internal displacements by a linear transformation

$$s(t) = UQ(t) \qquad (4.7)$$

The standard normal-mode analysis (Goldstein, 1950) allows one to determine the normal frequencies $\omega_j$, as well as the vectors

$$\vec{d}_{ej} = \sum_i \vec{A}_{ei}\, U_{ij}$$

of the transformation from normal displacements to the $u_e$ displacements

Since the normal modes are independent, the vibrational TCF factors into a product of correlation functions for each mode as shown below:

$$F_{v\vec{K}}(t) = \prod_{j=1}^{N_v} \langle\langle \exp[\, i\vec{K} \cdot \vec{C}_{aj} Q_j(0)] \times \exp[i\vec{K} \cdot \vec{C}_{aj} Q_j(t)] \rangle\rangle_v \quad (4.7)$$

The correlation of each mode is readily evaluated by means of the algebra of creation and annihilation operators $a_j^\dagger$ and $a_j$ (Messiah, 1961), through

$$\bar{Q}_j = [\hbar/(2\omega_j)]^{1/2} (a_j + a_j^\dagger) \quad (4.8)$$

Introducing the notation

$$I_{\theta j} = \sum_\xi (x_\xi / x) \left(\frac{\hbar}{2\omega_j}\right)^{1/2} C_{a\xi,j} \,, \quad (4.9)$$

where $\xi$ denotes the cartesian coopenent (x,y, or z) and using Eq (4.8) into Eq (4.7), we can write

$$F_{v\vec{K}}(t) = \prod_{j=1}^{N_v} \tilde{F}^{(j)}_{v\vec{K}}(t) \,, \quad (4.10a)$$

$$F^{(j)}_{v\vec{K}}(t) = \langle\langle \exp[-iKI_{aj}(a_j + a_j^\dagger)_0]$$

$$\times \exp[iKI_{aj}(a_j + a_j^\dagger)_t] \rangle\rangle_v \quad (4.10b)$$

By following a previous procedure (Micha, 1979b), one then arrives at

$$F^{(j)}_{v\vec{K}}(t) = \sum_{\theta_j} \exp(-in_j\omega_j t)\, \rho_{n_j} \,, \quad (4.11a)$$

$$\rho_{n_j} = \exp(-n_j a_j - X_j \cosh a_j)\, I_{n_j}(X_j) \,, \quad (4.11b)$$

$$X_j = \hbar(K C_j \cos\beta_j)^2/(2\omega_j \sinh\theta_j) \,, \quad (4.11c)$$

$$\theta_j = \hbar\omega_j/2k_B T \,, \quad (4.11d)$$

where $n_j$ is the number of quanta transferred into a mode of energy $\hbar\omega_j$, $I_{n_j}(X_j)$ is the modified Bessel function, $\beta_j$ is the angle between $\vec{k}$ and the vector $\vec{c}_j$, and $k_B$ is Boltzmann's constant. The total vibrational correlation function $F_{vK}$ in Eq. (4.10) can be rearranged as a sum of products of exponentials

$$F_{vK}(t) = \sum_{\underline{n}} \exp(-i\underline{n}\underline{\omega}_v t)\, F_{\underline{n}}(\vec{k}) \quad , \tag{4.12a}$$

$$F_{\underline{n}}(\vec{k}) = \prod_j F_{n_j} \quad , \tag{4.12b}$$

where $\underline{\omega}_v$ and $\underline{n}$ are column matrices with elements $\omega_j$ and integers $n_j$, respectively. It is immediately seen that the Fourier transform of the vibrational TCF would consist of a group of $\delta$-function peaks located at $\omega = \hbar\underline{n}\underline{\omega}_v$.

## 4.2 Short Time Expansion

The calculation of the vibrational TCF given in Eq. (4.10) can be simplified whenever the vibrational modes of the target satisfy $\hbar\omega_j \leq k_B T$. Therefore, one can approximate $F_v^{(j)}$ by a short time expansion around $t = 0$ (Micha, 1981), of the form

$$\ln F(t) = \ln F(0) + t\, \dot{F}(0)/F(0) + \tfrac{1}{2}\, t^2 [\ddot{F}(0)/F(0) - \dot{F}(0)^2/F(0)^2] \quad , \tag{4.13}$$

where a dot signifies a time derivative. Performing the derivatives from Eq. (4.10), the expression for each of the low frequency modes j is given by

$$\ln F_v^{(j)}(t) = it\Delta_j/\hbar - t^2\, \Gamma_j^2/\hbar^2 \quad , \tag{4.14a}$$

$$\Delta_j = \hbar\omega_j\, X_j \sinh \alpha_j \quad , \tag{4.14b}$$

$$\Gamma_j^2 = (\hbar^2\omega_j^2 X_j \cosh \alpha_j)/2 \qquad (4\text{-}14c)$$

where $X_j$ and $\alpha_j$ are the same quantities as given by Eq. (4-11). Collecting all the low frequency mode contributions one obtains the final expression

$$\ln F_v(t) = it \sum_j \Delta_j/\hbar \quad t^2 \sum_j \Gamma_j^2/\hbar^2 \qquad (4\text{-}15)$$

The Fourier transform with respect to time of Eq. (4-15) gives a Gaussian distribution peaking at the energy transfer $\varepsilon = \sum_j \Delta_j$ with a width $\Gamma = \sum_j \Gamma_j$. Both quantities would increase with momentum transfer.

## 4.3 Statistical Model for Single and Double Collisions

When an atom collides with a molecular adsorbate it causes transitions among the target's vibrational states. The most likely event is excitation of both adsorbate and substrate vibrations, although deexcitation is also possible from the thermally populated excited states of the target.

The mechanism of energy transfer depends on the scattering angle, $\Theta$, defined as the angle between the incoming and outgoing momentum vectors. For an atom approaching along the perpendicular to the surface with a small impact parameter, b, collisions with the O atom of the adsorbate will lead to deflections by an angle larger than $\pi/2$, in which case only one encounter takes place. This can be seen in Figure 4-1, which has been drawn using covalent atomic radii plus a van der Waals radius for Ne atoms. If, however, the impact parameter is large, the first deflection is smaller than $\pi/2$ and the

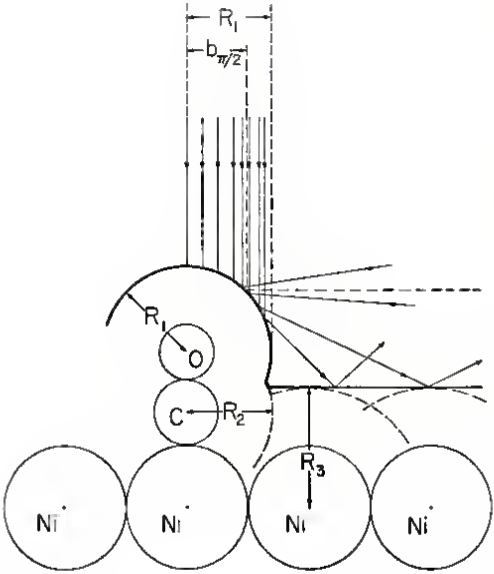


Figure 4.1: Trajectories showing regions of single and double collisions. Model drawn using covalent atomic radii plus a van der Waals radius for He atoms

etee next collidee with the surface befote fiying eway et an angle lerger then π/2. Hence, the deflection function of such a collisfon would show two branches for θ > π/2. It is then obvious that an atee which hod been deflected by either mechanism could be detected at the same final scattering angle. Therefore, to obtain the double differentiol cross section one needs to add all contributions involving the same amoent of energy tranefer aed having the same ecattering angles regordless of the mechanism by which this occurred. In Chapter 2 an expreseion for the double differential cross section, for single collisiona and ander the impulse approximation, was shown to be given in terms of tha TCF. Using the vibrationel TCF obtained in section 4.1, one can write

$$\frac{d^2\sigma}{d\varepsilon d\Omega} = \left(\frac{d\sigma}{d\Omega}\right) \int \frac{dt}{2\pi\hbar} e^{-i\varepsilon t/\hbar} \sum_{\underline{n}} \exp(-in\underline{\omega}_v t)\, P_{\underline{n}}(\vec{k}) \quad . \tag{4.16}$$

Here one can recognize twa factars, the first, (dσ/dΩ), is an effective clessicel cross-section and the second has the meaning of a prebehility per unit energy. Then equation (4.16) can be rewritten as

$$\frac{d^2\sigma}{d\varepsilon d\Omega} = \left(\frac{d\sigma}{d\Omega}\right)\left(\frac{dP}{d\varepsilon}\right) \quad , \tag{4.17a}$$

where

$$\frac{dP}{d\varepsilon} = \int \frac{dt}{2\pi\hbar} e^{-i\varepsilon t/\hbar} \sum_{\underline{n}} e^{in\underline{\omega}_v t} P_{\underline{n}}(\vec{k}) = \sum_{\underline{n}} dP_{\underline{n}}/d\varepsilon \tag{4.17b}$$

In particular, for a ecattering chereclerized by the energy transfer ε = nħω, we find the partial differential cross section to be given by

$$\frac{d^2\sigma_{\underline{n}}}{d\varepsilon d\Omega} = \left(d\sigma/d\Omega\right)\left(dP_{\underline{n}}/d\varepsilon\right) \qquad (4.17)$$

This way, the total differential [illegible] by

$$\frac{d^2\sigma}{d\varepsilon d\Omega} = \sum_{\underline{n}} \left(d\sigma/d\Omega\right)\left(dP_{\underline{n}}/d\varepsilon\right) \qquad (4.18)$$

A detailed cross-section should account for the quantal phase interference of branches I and II. However, in our case we must average the detailed cross sections over the target thermal distribution, which would lead to cancellation of the interference term except possibly near $\theta = \pi/2$. Denoting the two branches corresponding to single and double collisions by I and II, respectively, we can then write the cross-section

$$\frac{d^2\sigma}{d\varepsilon d\Omega} = (d\sigma/d\Omega)^{(I)}\,(dP/d\varepsilon)^{(I)} + (d\sigma/d\Omega)^{(II)}\,(dP/d\varepsilon)^{(II)} \qquad (4.19)$$

where the first term is obtained from branch I at angle $\theta$, and the second term from branch II at the same angle.

The probability per unit energy transfer corresponding to single collisions, $(dP/d\varepsilon)^{(I)}$, follows directly from the Fourier transform of the vibrational CCF given by Eq. (4.16). The second term in Eq. (4.19) is more difficult to obtain because it is a combined probability since it accounts for the transfer of two amounts of energy occurring in a double collision. They are the energy $\varepsilon^{r}$ transferred during the first collision into the cluster plus the amount $\varepsilon^{0}$ transferred during the second collision into the metal away from the adsorbate. This term can be derived using statistical arguments as follows. We first separate the collection $\underline{n}$ of normal mode quantum numbers of the whole target into the subsets $\underline{e}^{c}$ for a

cluster and $\underline{n}^m$ for the metal surface away from the adsorbate. The latter contains the parallel and perpendicular vibrational modes of the clean surface. For the double collisions we then write

$$(dP/d\varepsilon)^{(II)} = \int \frac{dt}{2\pi\hbar} e^{i\varepsilon t/\hbar} \sum_{\underline{n}} e^{iE_{\underline{n}} t/\hbar} P_{\underline{n}}(\varepsilon) , \qquad (4.20a)$$

$$P_{\underline{n}}(\varepsilon) = \int_0^1 dy\ P_{\underline{n}^c}(y\varepsilon)\ P_{\underline{n}^m}[(1-y)\varepsilon] , \qquad (4.20b)$$

where $E_{\underline{n}} = \sum n_j \hbar\omega_j$ and $P_{\underline{n}}$ is the probability of transferring $\underline{n}$ quanta when the total energy transfer is $\varepsilon = \varepsilon^c + \varepsilon^m$. The probability $P_{\underline{n}}$ has been written as the convolution of the probabilities $P_{\underline{n}^c}$ and $P_{\underline{n}^m}$ for excitation of the cluster and the clean surface, corresponding to a sequence of two independent events. The integration variable y in Eq. (4.20) is defined by $y = \varepsilon^c/\varepsilon$. Using $E_{\underline{n}} = E_{\underline{n}^c} + E_{\underline{n}^m}$ we then find

$$(dP/d\varepsilon)^{(II)} = \int \frac{dt}{2\pi\hbar} e^{-i\varepsilon t/\hbar} \int_0^1 dy\ F^c(t,y)\ F^m(t,1-y) , \qquad (4.21a)$$

$$F^c(t,y) = \sum_{\underline{n}^c} \exp(iE_{\underline{n}^c} t/\hbar)\ P_{\underline{n}^c}(y\varepsilon) , \qquad (4.21b)$$

$$F^m(t,1-y) = \sum_{\underline{n}^m} \exp(iE_{\underline{n}^m} t/\hbar)\ P_{\underline{n}^m}[(1-y)\varepsilon] \qquad (4.21c)$$

Here, $F^c(t,y)$ and $F^m(t,1\ y)$ are the vibrational TCFs for the cluster and clean metal respectively. Each of these two TCFs could be calculated from the expressions in Eq. (4.11)

However, it is usually found, as was the case in Chapter 3 for a CO molecule adsorbed on a Nickel surface, that frequencies can be separated into high and low ones. Thus, for each low frequency mode, l, one can use the short time expansion given in Eq. (4.14) which, when replaced in Eq. (4.21), leads to

$$\left(\frac{d^2\sigma}{d\varepsilon\, d\Omega}\right)^{(II)} = \sum_{n_f} \frac{d^2\sigma_{n_f}}{d\varepsilon\, d\Omega}\,, \tag{4.22a}$$

$$\frac{d^2\sigma_{n_f}}{d\varepsilon\, d\Omega} = \left(\frac{d\sigma}{d\Omega}\right)^{(II)} \int_0^1 dy\; P_{n_f}(y)$$

$$\times \left(\frac{\pi}{\Gamma^2}\right)^{1/2} \exp\left[\,(\varepsilon_s - \Delta)^2/(2\Gamma^2)\right]\,, \tag{4.22b}$$

where $n_f$ is the number of quanta gained by the fast mode of energy $\hbar\omega_f$, and $\varepsilon_s = \varepsilon + n_f\hbar\omega_f$ is the energy gained by the slow modes. The total shift $\Delta$ and width $\Gamma^2$ are sums over all slow modes l and are functions of l-y.

Equation (4.22) may then be used to calculate double differential cross-sections (DDCS) versus the scattering angle $\theta$, and versus the amount of energy $\varepsilon_s$, transferred into the slow modes, for each fast mode $n_f$.

# CHAPTER 5
# GAS-ADSORBATE INTERACTIONS POTENTIALS: EFFECTIVE DIFFERENTIAL CROSS-SECTIONS

In previous chapters we have shown that double differential cross-sections for atom-adsorbate collisions can be obtained from a product of deflection probability and a target absorption probability, where the former can be given by an effective differential cross section. In order to obtain this effective differential cross section one must first specify an interaction potential between the projectile and the target. In this chapter we first review general qualitative features of the atom surface interaction potential and the usual procedure one can follow to obtain analytic representations which are desirable for scattering calculations. Since not much is known quantitatively about the behavior of the potential, one is forced to introduce model potentials.

A model potential is then presented for the interaction between helium atoms and lithium ions with a carbon monoxide molecule adsorbed on a metal surface.

These model potentials are then used in trajectory studies of the two systems, $He$ - adsorbed CO molecule and $Li^+$ - adsorbed CO molecule, to obtain the desired effective differential cross sections.

## 5.1 Atom (Ion)-Adsorbate Interaction Potential

The general features of gas-adsorbate potentials are expected to be similar to the qualitative picture of the gas-surface potentials. In the case of sufficiently small distances from the surface the potential has a strong repulsive part in front of the solid. The reason for this repulsion is the overlapping of the wave functions of the electrons of the gas atom and of the electrons at the surface of the solid. This gives rise to a periodic modulation of the repulsive part of the potential parallel to the surface. At longer distances the gas-surface potential is dominated by an attractive van der Waals interaction given by the distance-dependent polarization energy between a gas atom and the solid. This attractive part of the potential is caused by the interaction of the gas atom with a relatively large number of crystal atoms, so that the attractive part can be assumed to be practically constant parallel to the surface.

There have been only a relatively small number of attempts to calculate the physical gas-surface interaction potential from first principles. Calculations of He on metals have been done (Zaremba and Kohn, 1977) to calculate the attractive van der Waals interaction of large distances and the repulsive interaction at small distances and to construct from these two parts a complete potential as a function of the distance Z of the gas atom from the surface. In this procedure the position of the reference plane $Z = Z_0$, from which the distance of the gas atom should be measured, appears as an essential parameter.

More recently, methods for generating surface potentials from surface electron densities have been presented. Some authors (Esbjerg and Norskov, 1980) have suggested a theory which gives a

relation of proportionality between the helium potential energy and the surface electron charge density. However, when experimental results are compared with theoretical predictions, they strongly disagree. In particular, for the Ni(110) surface the corrugation parameter across the close-packed rows is found to be three times the experimental value (Annett and Haydock, 1984). Similarly, several ab initio calculations of potentials for weakly corrugated surfaces have not been very successful, predicting approximately two times too large a corrugation (Hutson et al., 1985). However, semi-empirical methods, allowing the adjustment of some parameter, have led to good agreement with the He scattering data (Harris and Liebsch, 1982b).

An approximation frequently used that allows calculating physisorption potential energies of gas-surface systems is based on the additivity assumption. The thermally averaged solid surface is assumed to have perfect periodicity and thus may be expressed in a Fourier expansion as follows:

$$V(\vec{r}) = \sum_{\vec{G}} v_{\vec{G}}(Z) \exp(i\vec{G}\cdot\vec{R}_S) , \qquad (5.1)$$

where $\vec{r} = (x,y,z) = (\vec{R}_S,Z)$, with the Z axis extending in the direction normal to the surface. The two dimensional vectors $\vec{G}$ are the reciprocal lattice vectors of the surface. The first term in the expansion, $v_{\vec{0}}(Z)$, is considered the over-all average potential and is the large potential in perturbation theory which causes specular diffraction. The $v_{\vec{G}}(Z)$ for $\vec{G} \neq 0$ are treated as perturbations which cause non-specular diffraction. Diffraction experiments give information on both the dimensions of the unit cell via the angular location of Bragg peaks and the distribution of the scattering centers within the unit cell via the intensities of diffracted beams.

However, to obtain a solution to the diffraction problem in closed form, the potentials $v_{\vec{G}}(Z)$, including $\vec{G} = \vec{0}$, must be simple

A convenient empirical representation of the $v_{\vec{G}}(Z)$ is the Morse/exponential repulsion representation (MERR) (Cunnean, 1987) which represents $v_{\vec{0}}(Z)$ by a Morse potential and $v_{\vec{G}}(Z)$ by an exponential repulsion for $\vec{G} \neq 0$

$$v_{\vec{0}}(Z) = D[\exp(-2\alpha Z) - 2\exp(-\alpha Z)] \ , \qquad (5.2a)$$

$$v_{\vec{G}}(Z)/D = K_{\vec{G}} \exp(-2\alpha Z) \quad \vec{G} \neq 0 \ , \qquad (5.2b)$$

where $K_{\vec{G}}$ are the so-called diffraction strengths. In the 4G model where only the four smallest nonzero reciprocal lattice vectors are used, the sum over $\vec{G} \neq 0$ reduces to four terms and the $K_{\vec{G}}$ reduces to a single value.

The qualitative picture of the gas surface interaction we have described has to be modified in the case of ion surface interactions. In these cases and at short distances, the important contribution to the surface interaction comes from the overlap of the electronic charge densities, which in the case of closed shell ions, is reasonably considered as purely repulsive. At large distances from the surface the interaction is attractive and is well described by the macroscopic image potential, $V_{im} = -e^2/4Z$. The image picture, however, loses validity when the particle approaches to within a few angstroms of the surface. Here again, as in the case of the van der Waals interaction, a parameter may be introduced to define the position of the image plane which improves the validity of the image potential.

Recently, a way to construct the interaction potential between an ion and a surface of a monatomic solid has been presented (Mann et al., 1987). The $K^+$ W(100) potential constructed this way was found

to agree with an empirical potential used to fit scattering data for the same system (Huipke and Mann, 1985)

The interaction of an atom with an adsorbate will be comprised of direct potentials (the attractive van der Waals and the repulsive short range), as occur in the gas phase, and of indirect surface-mediate potential which arise due to the proximity of a third polarizable body whose presence modifies the simple, two-body gas phase interaction The surface-mediated potential is expected to be of particular importance in the case of long range interactions and only for the case of low incoming atom energies

The induced polarization interaction of closed shell atoms with anisotropic adsorbed molecules has been investigated and a theory of the long range van der Waals potentials acting between a He atom and a CO molecule adsorbed on a metal surface has been presented (Lin and Gushalter, 1987), and the full potential has been given as the sum of the long range interaction plus the short range repulsion for the atom gas phase CO molecule interaction

A simple approach to the full description of an atom adsorbate interaction consists in superimposing an ab initio atom-gas phase molecule interaction potential on an empirical atom-surface potential This procedure has been used in the system He/OC-Pt(111) (Lahee et al., 1987) and has been found to give good agreement with the experimentally predicted classical turning points.

5.1.1 He/OC-Ni(001) Interaction Potential

Since our final goal is to obtain an interaction potential simple enough to be used in trajectory studies, we follow the assumption that the atom-adsorbate potential can be given by superimposing an atom-molecule potential on an atom surface potential.

For the atom-surface potential we have followed the procedure given by Harris (Harris and Liebsch, 1982a). Basically, their theory, a generalization of that used for jellium surfaces (Zaremba and Kohn, 1977), relates the interaction to shifts of the band energies due to the presence of the helium. In this theory, the Hartree-Fock interaction energy to lowest order in the overlap is given by

$$V_R(\vec{r}) = \int_{-\infty}^{\epsilon_F} d\epsilon\, \rho(\epsilon,\vec{r})\, g(\epsilon) \ , \qquad (5\text{-}3)$$

where $\epsilon_F$ is the Fermi energy, $g(\epsilon)$ is a smooth function of energy and $\rho(\epsilon,\vec{r}_N)$ is the local density of states at the helium nucleus. In the case of face centered cubic (fcc) transition metals

$$V_R(x,y,z) = V_0\, e^{-\alpha z}\left\{1 + \frac{\alpha h_0}{2}\exp\left[-\beta(z-z_0)\right]h(x,y)\right\} \ , \qquad (5\text{-}4a)$$

$$h(x,y) = \cos(g_x x) + \cos(g_y y) \ , \qquad (5\text{-}4b)$$

$$\alpha = 2[2(w+\Delta)]^{1/2} \ , \qquad (5\text{-}4c)$$

$$\beta = \left[2(w+\Delta) + g_x^2 + g_y^2\right]^{1/2} \qquad \frac{\beta}{2} > \alpha \qquad (5\text{-}4d)$$

Where $w$ is the work function of the metal, $\Delta$ is an energy shift that depends primarily on the band width, and $g_x$, $g_y$ are the magnitudes of the smallest reciprocal vectors in the x and y direction, respectively.

The attractive part of the helium interaction is taken to be given by the van der Waals expression $-C_{vw}(z-z_{vw})^{-3}$ with the origin of z lying one-half a layer spacing outside the topmost plane of nuclei.

The full He-adsorbate potential can then be written as the sum of the three contributions: repulsive He - surface, attractive He - surface and He - gas phase molecule, that is:

$$V(x,y,z) = V_\phi(R_a) + V_{rep}(R) + V_{vw}(z) \quad , \tag{5.5a}$$

$$V_\phi(R_\phi) = A_a \exp(-B_a R_a) \quad , \tag{5.5b}$$

$$V_{rep}(R) = V_s(z) + V_{corr}(x,y,z) \quad , \tag{5.5c}$$

$$V_s(z) = A_s \exp(-B_s z) \quad , \tag{5.5d}$$

$$V_{corr}(x,y,z) = V_s(z)\, h(x,y,z) \quad , \tag{5.5e}$$

$$h(x,y,z) = \delta_s D \exp[-\beta(z-z_0)]h(x,y) \quad , \tag{5.5f}$$

$$V_{vw}(z) = -C_{vw}/(z-z_{vw})^3 \quad , \tag{5.5g}$$

where $R_a$ represents the distance between the He atom and the oxygen atom of the adsorbed CO molecule and it can be written as

$$R_\phi = [R^2+R_m^2 - 2R_m R\cos\theta]^{1/2} \quad ,$$

and $R_m$ is the distance between the surface and the oxygen atom in the CO molecule. In the case of CO on Ni(001), $R_m$ has been determined experimentally (Andersson and Pendry, 1980). The geometry of the problem is given in Fig. 5.1, where the surface defines the (x,y) plane and the z coordinate is perpendicular to the surface and passes through the center of the adsorbed molecule.

From electronic calculations of CO on a cluster of surface atoms there is overwhelming evidence that there is a chemical bond formation between the substrate valence band orbitals and the adsorbed CO valence molecular orbitals. The CO $5\sigma$ molecular orbital may acquire partial metal character and thereby donate some of its electronic charge into the metal states. Simultaneously, some of the metal charge may be back donated into the formerly unoccupied CO $2\pi^*$

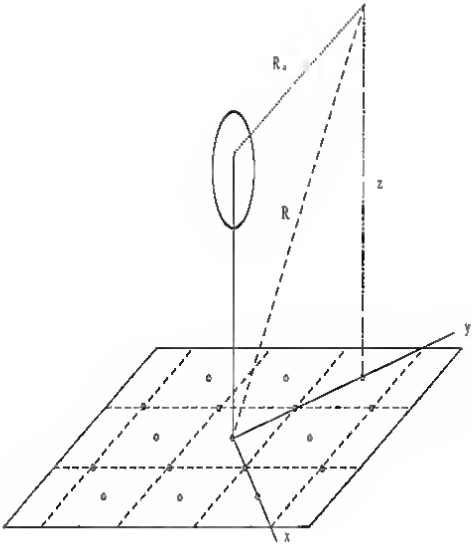


Figure 5 1: System of coordinates and geometry used for the interaction potential a) On top model; b) Bridge model.

molecular orbital which may become a bonding one with respect to the metal-CO interaction (Blauschlicher, 1986). This back donation into the $2\pi^*$ orbital is then responsible for the weakening of the molecular bond and an increase of the CO bond length. The C-O bond length in a CO molecule is 1.128 Å, whereas in a $CO_2$ molecule, it is 1.159 Å which is closer to the value found in carbonyl compounds and in a CO molecule adsorbed on a Nickel surface.

In view of the above arguments, we have chosen to use the parameters given by the fitting of a SCF interaction potential energy for He - $CO_2$ (Clary, 1982), for the He - adsorbate repulsive part of the potential. Diffraction data have not been reported on the He Ni(001) system, so we have used the Harris and Liebsch parameters for the He surface interaction. A list of all the parameters we have used in this work is given in Table 5.1 for the case of a CO molecule adsorbed on top. The only parameter which changes when one considers the bridge bonding situation is the height of the adsorbed molecule. This has been chosen according to the geometric parameters of the clusters presented in Chapter 3.

It is known from the study of atomic and molecular interactions that the van der Waals interactions must be damped at short distances, because of electronic overlap of wave functions. In order to accomplish this damping, we have used a function of the type $f(z) = \exp[\beta(z-z_0)]/(1 + \exp[\beta(z-z_0)])$ which for $z<z_0$ goes smoothly to zero.

The interaction potentials for the on top and bridge case are shown in figures 5.2 and 5.3, respectively. It can be seen that in both cases the interaction is steeply repulsive in the region of hyperthermal energies, i.e., $\geq 1$ eV, in which we are interested. The

Table 5-1 Interaction Potential [illegible] He/OC Ni(001)

| | [illegible] | He/Ni |
|---|---|---|
| $A_s$(eV) | 7157.29 | |
| $\beta_s$($Å^{-1}$) | 4.13 | |
| $A_z$(eV) | | 12.0 |
| $\beta_z$($Å^{-1}$) | | 2.63 |
| D(Å) | | 0.0127 |
| $\beta$($Å^{-1}$) | | 0.8692 |
| $C_{vw}$(eV$Å^3$) | | 0.22537 |
| $z_0$(Å) | | 3.01644 |
| $z_{vw}$(Å) | | 0.24396 |
| $g$($Å^{-1}$) | | 2.489 |

Figure 5.2 Attractive ( ) and full (——) potential for the on top He/OC-Ni(001) system over the surface point x=y=0 The inset shows the region around the minimum.

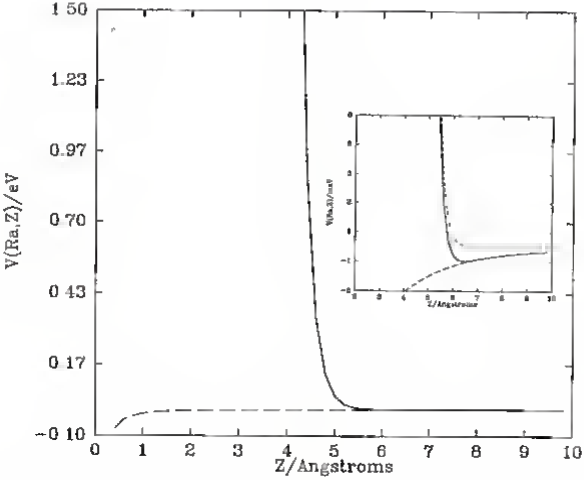
1.50
1.23
0.97
0.70
0.43
0.17
-0.10
V(Ra,Z)/eV
0
1
2
3
4
5
6
7
8
9
10
Z/Angstroms

Figure 5.3: Attractive (---) and full (——) potential for the bridge He/OC-Ni(001) system over the surface point x=y=0. Inset shows region around the minimum.

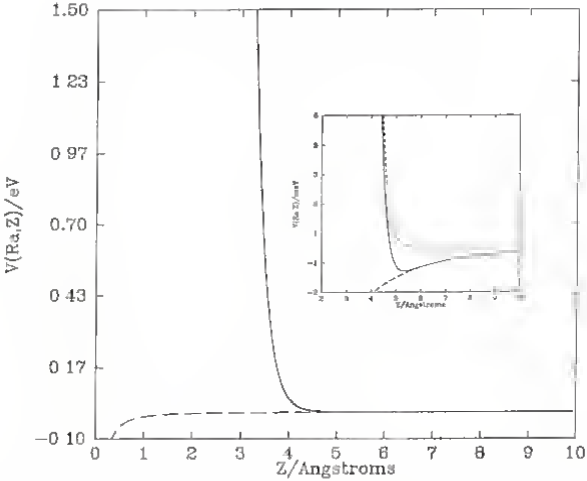
1.50
1 23
0 97
0.70
0 43
0 17
−0 10
V(Ra,Z)/eV
0
1
2
3
4
5
6
7
8
9
10
Z/Angstroms

interaction for the on-top case gives a larger turning point than the case of the bridge, as was expected due to the shorter distance of the CO molecule to the surface in the latter case. It also can be seen in the inset of both figures that the bridge potential presents a deeper well than the top potential. This is because the attractive part of the interaction between the He atom and the surface is stronger when the He atom is over the space between two surface atoms, rather than directly on top of a surface atom, and in the bridge model, the adsorbate is positioned in between two surface atoms.

In figures 5.4 and 5.5, the dependence of the potential in the (y,z) plane is shown for the two models. Again the bridge gives larger turning points than the top model but now the effect of the adsorbate becomes smaller as one moves away from it and finally, when $y \geq a$, the two models give identical turning points. This is due to the fact that for $y \geq a$ one is only seeing the He - surface interaction.

5.1.2 $Li^+$/OC-Ni(001) Interaction Potential

The ion-adsorbate interaction potential can in general be written as the sum of three contributions: the ion molecule repulsive interaction, the ion-surface interaction, and the image interaction. As was mentioned in Sect. 5.1, a recent approach to construct the interaction potential between an ion and the surface of a monatomic solid (Mann et al., 1987) is found to agree with an empirical potential used to fit scattering data for the system $Li^+$/W(001) (Hnipke and Mann, 1985). We have chosen to represent the $Li^+$ Ni(001) potential by a modified MEER potential which has been used to fit scattering data for the system $Li^+$/Ni(001) (Gerlach and Hulpke,

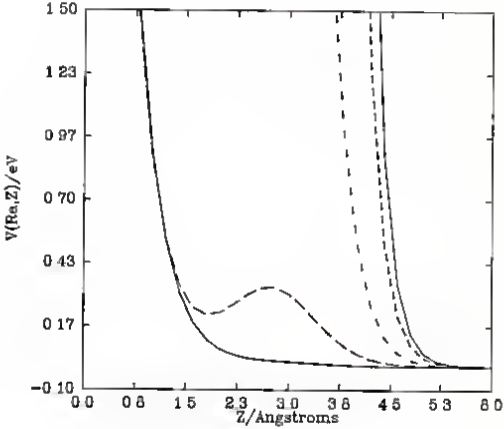


Figure 5 4 Potential for on-top He/OC-Ni(001) system over several points on the (y z) plane. Starting from first line on the right, the points correspond to y=0, a/4, a/2, 3a/4, a, where a is the lattice spacing

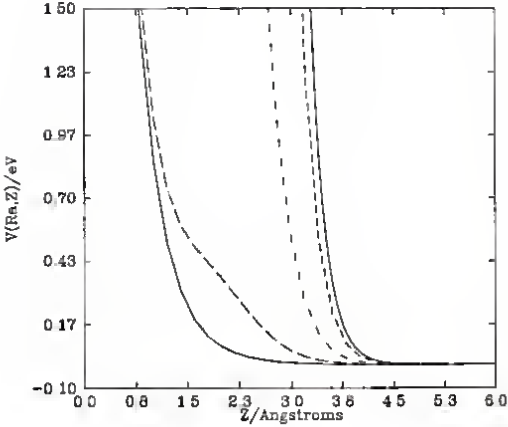


Figure 5.5 Potential for bridge Ho/OC Ni(001) system over several points on the (y-z) plane. Starting from first line on the right, the points correspond to y=0, a/4, a/2, 3a/4, a; where a is the lattice spacing

1977) Here again a [illegible] is [illegible]

$$V(x,y,z) = V_a(R_a) + V_s(R) + V_{image}(z) \qquad (5.6)$$

The term $V_a(R_a)$ is identical to the one for the helium potential but now the parameters are obtained from $Li^+/CO_2$ data (Vilkliengs and Micha, 1983a). The term $V_s(R)$ contains a repulsive and an attractive term given by

$$V_s(R) = V_{rep}(z) + V_{attr}(x,y,z) \qquad (5.7a)$$

$$V_{rep}(z) = A_e \exp(-B_s z) \qquad (5.7b)$$

$$V_{attr}(x,y,z) = D\{\exp[-2\beta(z-z_1)][-2\exp[\beta(z-z_1)]] \qquad (5.7c)$$

$$+ 2\exp[-2\beta(z-z_1)]\}\, h(x,y) \qquad (5.7c)$$

and

$$V_{image}(z) = -e^2/4(z-z_0) \qquad (5.7d)$$

The parameter D represents the well depth and $\beta$ its width. The meaning of each of these terms has already being explained in Section 5.1. However, one should mention that in this model the Coulomb term, at sufficiently small distances z from the surface, is cancelled by the repulsive part included in $V_{attr}$. The potential parameters used for the $Li^+/OC\ Ni(001)$ system are presented in Table 5.2. The shape of the potential calculated from this construction is again found to be steeply repulsive around the energies of interest which in this case are 10 to 50 eV. Figures 5.6 and 5.7 show the potentials for the top and bridge model respectively. One can observe that the trends for turning points and well depths, when compared between models, are the same as the ones found for the He potential. However, an important difference in the behaviour of the potential in the y-z plane can be found when one compares the two

Table 5.2 Interaction Potential Parameters for $Li^+$/OC Ni(001)

| | $Li^+$/CO | $Li^+$/Ni(001) |
|---|---|---|
| $A_R$(eV) | 1777.55 | |
| $B_R$($Å^{-1}$) | 5.27 | |
| $A_S$(eV) | | 2400.0 |
| $B_S$($Å^{-1}$) | | 3.0 |
| D(eV) | | 1.0 |
| $\beta$($Å^{-1}$) | | 1.1 |
| $\alpha$ | | 0.1 |
| $z_0$(Å) | | -0.75 |
| $z_1$(Å) | | 0.50 |

Figure 5.6 Attractive (– – –), Repulsive ( --) and full (——) potential for the on-top $Li^{+}$/OC Ni(001) system over the surface point x=y=0. Inset shows region around minimum

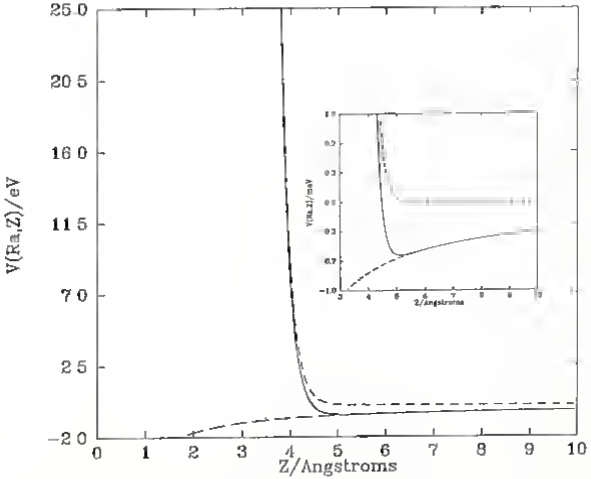
25.0
20.5
16.0
11.5
7.0
2.5
-2.0
V(Ra,Z)/eV
0
1
2
3
4
5
6
7
8
9
10
Z/Angstroms

Figure 5.7 Attractive (– – –), Repulsive (——) and full (——) potential for the bridge $Li^+$/OC-Ni(001) system over the surface point X=y=0 Inset shows region around minimum

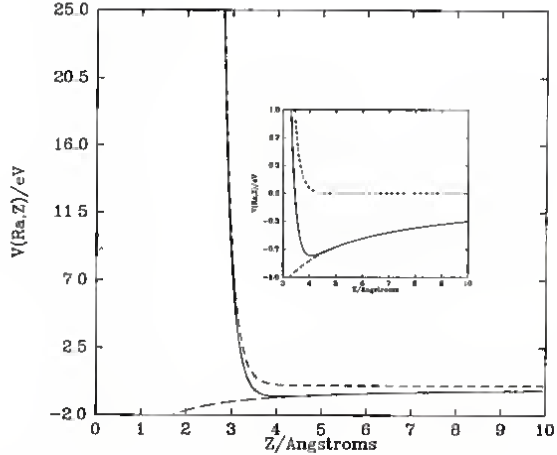
25.0
20.5
16.0
11.5
7.0
2.5
-2.0
V(Ra,Z)/eV
0
1
2
3
4
5
6
7
8
9
10
Z/Angstroms

different systems. In figures 5.8 and 5.9 for the $Li^+$/OC Ni(001) system, one can observe that the turning points, as one moves away from the adsorbate, do not change as much as they do in the He/CO Ni(001) system. This is because the $Li^+$-Ni(001) interaction is more attractive on top of the surface atoms than in between atoms, this is the opposite of what occurs for the He-Ni(001) interaction.

## 5.2 Effective Classical Differential Cross-Sections

The interaction potential in the system atom(ion)-adsorbate surface is not only dependent on the separation between the atom and the adsorbate but also depends on the separation between the atom and the surface. This represents a two center interaction problem, which means that the problem is not of a central force type and the classical cross sections can not be evaluated from the formulation for isotropic potentials.

For anisotropic potentials, the differential classical cross sections can be evaluated from a classical trajectory $\vec{R}(t)$ determined by

$$M \frac{\partial^2 \vec{R}}{\partial t^2} = \frac{\partial V}{\partial \vec{R}} \qquad (5.8)$$

To obtain the differential cross-sections one needs to go from an initial element of area determined by the impact parameter, b, and the initial azimuthal angle, $\phi_0$, to a final element of area determined by the final polar, $\theta$, and azimuthal, $\phi$, angles. Therefore, one needs the transformation from the set $(b,\phi_0)$ to the set $(\theta,\phi)$. This transformation is obtained by the Jacobian and the differential cross-section (Villalonga and Micha, 1987) is then given by

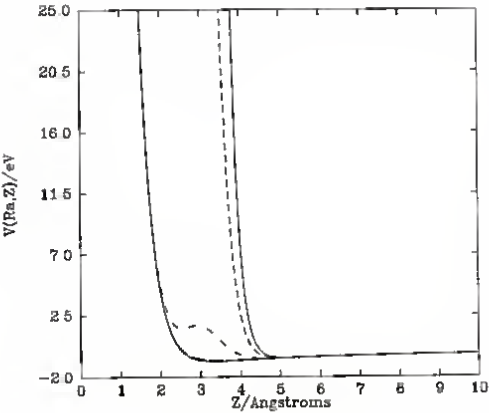


Figure 5.8 Potential for on top $Li^+$/OC Ni(001) system over several points on the (y-z) plane. Starting from solid line on the right the points correspond to y=0, a/4, a/2, 3a/4, a, where a is the lattice spacing.

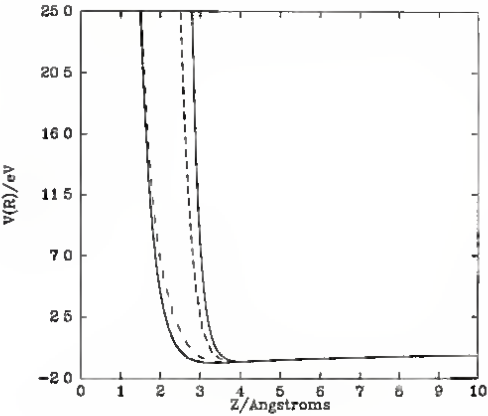


Figure 5 9 Potential for bridge $Li^+$/OC-Ni(001) system over several points on the (y-z) plane Starting from solid line on the right the points correspond to y 0- a/4, a/2, 3a/4, a, where a is the lattice spacing

$$\frac{d\sigma_c}{d\Omega} = (b/\sin\theta)\left|\frac{\partial(b,\phi_0)}{\partial(\theta,\phi)}\right| \qquad (5.9)$$

The above procedure involves a significant amount of computing time. In order to reduce the computational efforts we have used a simplified procedure based on histogram methods which have been widely used in the computation of elastic and inelastic and inelastic molecular differential cross-sections (Gentry, 1979).

In physical applications of scattering by adsorbates we are concerned not with the deflection of a single particle but with the scattering of a beam of identical particles, with a specified kinetic energy, $E_i$, striking a sample of the material under study. The atoms in the beam have different impact parameters and are scattered through different azimuthal and polar scattering angles.

Using a bundle of trajectories, the density of the incident beam can be represented by the ratio of the number of impinging trajectories, $dN_i$, over an area dxdy of the sample. In conditions of normal incidence, that is, for an initial angle $\theta_i = 0$ deg. measured from the normal to the surface under study, the area dxdy, can be represented by a grid of $(x_i, y_i)$ points. These points are related to the initial conditions, $(b, \phi_0)$, of the trajectories by $x = b\cos\phi_0$ and $y = b\sin\phi_0$. Denoting by $dN_f$ the number of trajectories with final scattering angles within the intervals $(\theta, d\theta)$ and $(\phi, d\phi)$, the differential cross sections may then be obtained from

$$d\sigma/d\Omega = (dN_f/\sin\theta\, d\theta\, d\phi)/(dN_i/dx dy) \qquad (5.10)$$

The quantity, $dN_f$, can be extracted from studies of trajectories by analyses of the final polar and azimuthal angles of the individual trajectories.

Ttejertories were obtained by numeriraiiy solving Hamiiton's equations in the coordinete system shown in Frg. 5 i. The set oi six first order differential equations was iotegrated by a wethed whirh nees e eodified form of the Adams Bece formuias and lersi extrepoietion (Sheepine end Gordon, 1975) The inrtiei rendirions ($b, \phi_0$, $K_{mex}$) were chosen by tequiring thet the intetertion potentrel be smaii with respect to the relative transiotional energy, e.g., by e ratio of $10^{-3}$, end the same rriterion wee used to terminate each individuei trajectory

The orea of the target sampled by the trajectories ia related to the maxieue iopact parametet, $b_{max}$, defined as the iergest impart petameter for which the trejertories show the rnfluenre of the adsorbate. The otee was rhosen to he grven by $\Delta x \Delta y$ where $\Delta x = x_{mex} - x_0$, and $x_{eax} = b_{eax} \cos\phi_0 (b_{eax})$. Here $\phi_0(b_{eax})$ is the initial ozimuthal ongle for which $b_{max}$ is found. This aethed viii essure thet the hundle of trajertories wili eample the region where the interartion betweea the projectile and the adsetbate is of impertenre.

In genetai, the trajertories behave differentiy according to three separate regions. The first region, for small impect parameters is where the trejecteties ore deflected mainiy by the strong repulsive ieterertion with the adsetbed meieruie. These trajectories can he sard to he srngle encounter coilisions. The second tegren is whete the trajecteries are deflected twice. The first deflection is caused by the interaction with the adsetbate and the second by the interertion wrth the snrface. These trajectories are double enrounter celiisiene. Frnaiiy, the thrrd region is whete the interertion is meiniy dne to the effect of the snriere. These

trajectories have impact parameters b[illegible] and do not stay in the same plane from large polar scattering angles where they originated. Energy conservation was checked at every step in the calculation and was kept to about 2%. Several of the trajectories were back integrated and always reproduced the initial values with an accuracy of at least two significant figures.

Calculations for lithium were done both with and without the effect of the image. The image effect appears to be of no significance for large deflections. Only trajectories with polar angles around 50° seem to be significantly affected. This can be seen in figure 5-10 where trajectories in the (x z) plane, for the $Li^+$ with 10 eV of energy are shown.

The trajectories show the shape and size of the adsorbate and, as was expected, they reflect the different sizes of the adsorbate in the two models, see figure 5-11.

In the case of helium atoms, the trajectories end at larger polar angles than the ones with similar impact parameters for lithium atoms, and trapping does not occur. This is due to the absence of the large attractive potential in the case of helium ions as compared to the one for lithium atoms.

The turning points are much larger for helium atoms than for the lithium ions. Compare Figures 5-10 and 5-12. This is to be expected, considering the difference in the kinetic energy of the two.

The dependence of the polar scattering angle on the impact parameter shows a minimum in all the cases, that is, for both projectiles and both models. This minimum corresponds to the impact parameter at which the separation between the regions of angle and

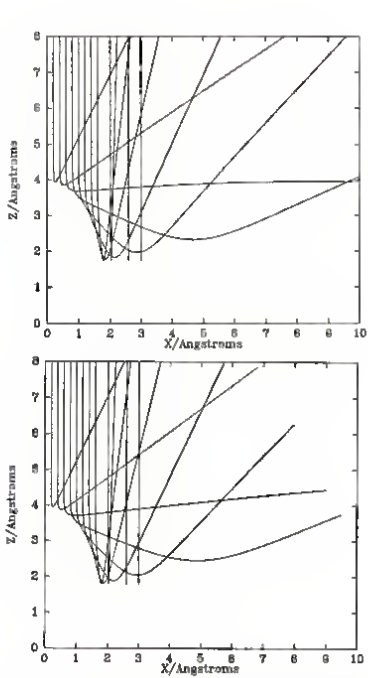


Figure 5-10: $Li^+$ trajectories in (x z) plane, on top model, for impact parameters b = 0-2, 0-4, . . ., 1-6, 2-0, 2-6, 3 0 Å; a) including image, b) without image

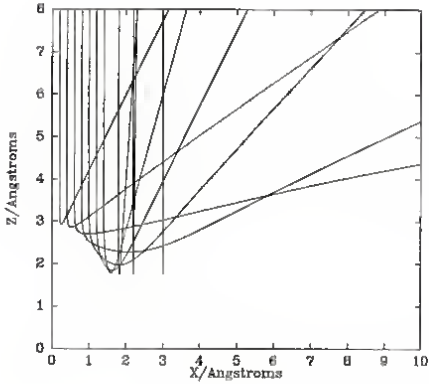


Figure 5.11: $Li^+$ trajectories in (x z) plane, bridge model, for impact parameters b = 0.2, 0.4, , 1.4, 1.8, 2.2, 3.0 Å.

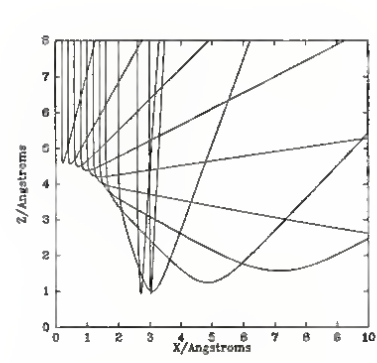


Figure 5.12: He trajectories in (x,z) plane for impact parameters b = 0.2, 0.4, ..., 1.6, 2.0, 2.6, 3.0 Å, a) On-top model. b) Bridge model

double encounters occurs. At large impact parameters, the deflection function reaches a maximum which indicates the beginning of the third region where the interaction is mainly between the projectile and the surface. These features are shown for the $Li^+$ ions in Figure 5.13 and for the He atoms in Figure 5.14. The corrugation appears to be larger in the case of the interaction with He.

The differential cross-sections for the on top model are presented in Figure 5.15 and Figure 5.16 for $Li^+$ and He atoms, respectively, for two different azimuthal angles. The main feature of these results is that the scattering is predominantly backscattering. In the case of $Li^+$ ions double collisions represent the main contribution for all scattering polar angles. The ratio of single to double contributions depends on the azimuthal angle. For lithium ions, the single collision contribution is the same for different directions on the x-y plane, but the double contribution is not symmetric with respect to the z axis. In the case of helium atoms, both contributions are angle dependent. A possible explanation for this is the larger corrugation present in the helium case. Also, one can notice that at certain azimuthal angles, e.g. $\Phi$=45°, the importance of single collisions with respect to double ones is reversed for certain ranges of point angles. This factor arises from the symmetry of the model. That is, the nearest neighbor distance along the y axis, $\Phi$=90°, is approximately 2.489 Å, whereas, in the direction with $\Phi$=45°, it is 3.52 Å, thus giving a larger double collision contribution for $\Phi$=45°.

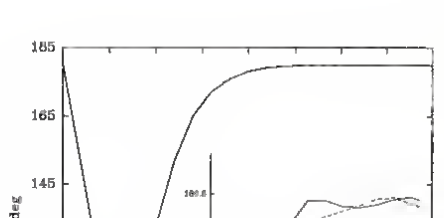


Figure 5.13: $Li^+$ deflection function, on top model. $\phi_0 = 0°$(——), 45°(---) The inset shows an enlargement for large impact parameters

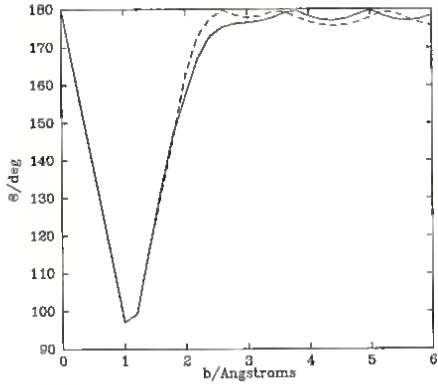


Figure 5 14 He deflection function, on-top model $\phi_0$ = 0°(——), 45°(---). The inset shows an enlargement for large impact parameters

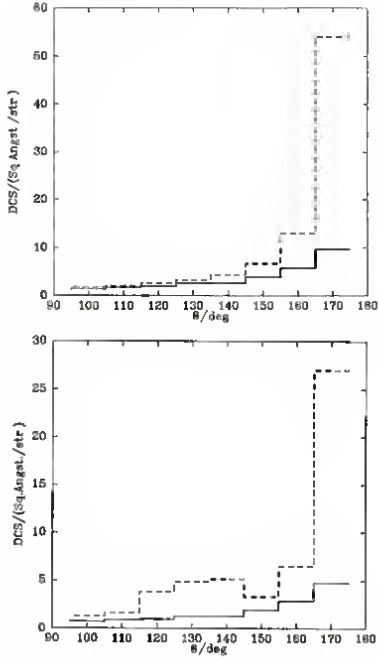


Figure 5.15: $Li^+$ differential cross-section, $d\sigma/d\Omega$, on-top model, for single (——) and double (– – –) collisions; a) $\Phi = 0°$ b) $\Phi = 45°$.

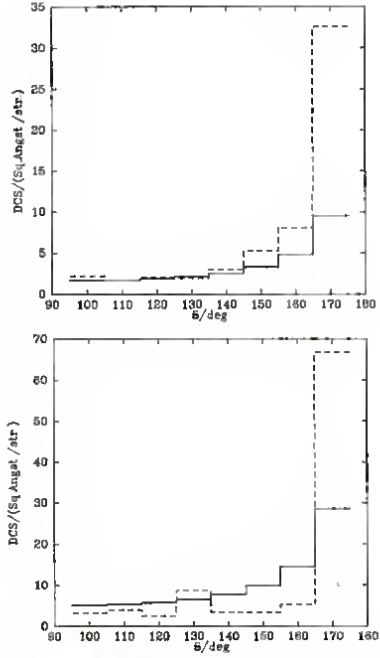


Figure 5.16 He differential cross section, $d\sigma/d\Omega$, on-top model, for single (——) and double (– – –) collisions, a) $\phi = 0°$ b) $\phi = 45°$.

# CHAPTER 6
# VIBRATIONAL ENERGY TRANSFER IN HYPERTHERMAL COLLISIONS OF He AND $Li^+$ WITH CO ADSORBED ON Ni(001)

In this chapter we apply the theoretical model presented in Chapter 4 to the scattering of He and $Li^+$ from a CO molecule adsorbed on a Ni(001) surface. We calculate double differential cross-sections for the energy and angular distributions of the He atoms and the $Li^+$ ions. Results are obtained for experimental conditions of high relative energy, 1 eV for He atoms and 10 eV for $Li^+$, for normal incidence and for the low coverages where the theoretical model is applicable.

## 6.1 Double Differential Cross Section for the System He/CO-Ni(001)

The calculations are based on the expressions obtained in Chapter 4 using the short time expansion of the vibrational TCFs for the low frequency modes of the target which, in our case, are all the surface and cluster modes except the CO stretch.

According to Eq. (4.22), the partial double differential cross-section for a given number of quanta, $n_f$, gained by the CO stretch will be given by a Gaussian distribution of energy transfer, with a shift $\Delta$ and width $\Gamma$, determined by the slow modes. This would be so for both mechanisms we are considering here, that is, for single and double collisions.

We have done the calculations considering single and double collisions. We find that single collisions are the predominant mechanism for helium scattering. In figures 6.1 and 6.2, the partial

differential cross section for excitation of the slow mode ($n=0$) are presented for the top and bridge model, respectively. In both cases the single collision contribution is larger than the double. The same is found to be true when energy is also transferred into the fast mode. This is shown in Figures 6.3 and 6.4 for $n=1$ and $n=2$, respectively, where it also can be seen that single collisions are even more predominant when a large amount of energy is transferred into the CO stretch.

Double differential cross-sections (DDCS) at scattering angles of $\theta=140$ and $\phi=0$ are shown, for the top and bridge models in Figures 6.5 and 6.6, respectively. In both cases the DDCS increase with increasing $\varepsilon$, which means with increasing $\varepsilon_0$, since $\varepsilon_f$ is fixed by $n$. As $\varepsilon$ is further increased, the DDCS goes through a maximum and then decreases to zero. In the case of no excitation of the CO stretch, that is, for $n=0$, there is no apparent difference between the two models. However, for excitation of CO by $n=1$, 2, and 3 quanta, the bridge model gives larger quantities for the DDCS and Gaussians centered at slightly smaller values of transferred energy. This is found to be in accordance with the fact that the frequency of the CO stretch in the bridge model is slightly smaller than in the top case and with equation (4.22) which tells us that the center of the Gaussian is given by $(\varepsilon_{n_f}+A)$.

We have also studied the angle dependence of the DDCS. Figures 6.7, and 6.8, and 6.9 present DDCS for the top and bridge models as a function of energy transferred for three different scattering angles, $\theta=100$, 140, and 170°, respectively. In both models the DDCS increases when the polar scattering angle increases. This trend is easily understood when one recalls that the CO stretch is a mode with

$A_1$ symmetry and motions perpendicular to the surface. Therefore, collisions at small impact parameters, leading to backward deflections, would be the most efficient to excite the CO stretch. It is also seen that the same trend is followed when n=0. In this case the overall process involves the simultaneous excitation of the slow modes, some of which are E type (motions parallel to the surface) and ions likely to be excited at small impact parameters, and some of which are A type and more likely to be excited. The two trends compound to give the resulting angle dependence which indicates that the A type modes are the dominant ones.

All the results presented and discussed up to now were obtained for a temperature of 300° K. The effect of the temperature on the probabilities of excitation for each mode is different and is determined by its magnitude in relation to the quantity $K_BT$. Modes whose frequencies satisfy $\hbar\omega_j >> k_BT$ will have excitation probabilities given by a Poisson distribution of $n_j$, independent of temperature for $T << \hbar\omega_j/k_B$. In our case, we find that the temperature dependence is due to the slow modes, whose frequencies satisfy $\hbar\omega_j \leq k_BT$, and is reflected in the width of the Gaussians. From equation (4.22) one obtains that the width at half-height is proportional to $\Gamma$ which is given by equations (4.14 and 4.11). These equations indicate smaller widths for smaller temperatures. In Figures 6.10, 6.11, and 6.12, we present DDCS for the top and bridge models at a temperature of 100° K for scattering angles $\theta$=0, and $\theta$=100, 140, and 170°, respectively. As expected, the peaks are narrower than the ones presented in Figures 6.7, and 6.8, and 6.9, which are obtained for a temperature of 300° K.

In the calculations for 100°K and at an angle of $\theta = 170°$, a very small peak appears in the region of very small energy transfer. In Figure 6.13 this peak is isolated and found to be centered at a point where the energy transferred, $\varepsilon$ is about 17 meV, and presents a Poisson, rather than a Gaussian, distribution. This seems to indicate that it corresponds to a mode with a frequency satisfying the minimum condition of $\hbar\omega_j > \varepsilon$ eV. In our analyses of normal modes we have modes corresponding to frustrated rotations with frequencies of 15.5 meV and 16.2 MeV in the bridge and top cases, respectively. This peak may then be associated with these modes, especially considering that it appears in both models.

Finally, the dependence of the DDCS with the azimuthal angle $\Phi$ for both top and bridge models is presented in Figures 6.14 and 6.15. The trends followed by the two models are essentially the same, with a smaller DDCS in the (110) direction ($\Phi$=0, 90°) than in the (100) direction ($\Phi$=45°). This result indicates that the projectile does not seem to notice the corrugation of the surface.

## 6.2 Double Differential Cross-Sections for the System $Li^+$/OC-Ni(001)

In the calculations for this system we have chosen energies in the range of 10 to 20 eV, which is considered an intermediate regime between low energy (thermal) and high energy, or Rutherford scattering, where the dynamics are rather simple. The calculations are based on the same formulation used for the He/OC-Ni(001). As before, we consider the separation of the modes into fast ones, that is the CO stretch, and slow modes, which are all the rest.

In this system, since the energy of the projectile is larger, more energy is available to be transferred into the target. As a consequence large values for the number of quanta transferred into the fast mode must be considered.

We first consider the partial double differential cross-sections as a function of energy transferred for a pair of scattering angles, $\Theta$ and $\Phi$. This is shown in the case of the top model and for $\Theta=100°$ and $\Phi=0°$ in Figure 6.16. In this case, contrary to what was obtained for He atoms, two peaks, well separated in energy, are found. The peak at high energies is found to originate from the double collision mechanism and the one at lower energies from single collisions. Double collision contributions are dominant for values up to n=10. As more energy is transferred into the fast mode, that is, for increasing values of n, the single collision starts to become more important. At this value of $\Theta$, the excitation of the CO stretch by v=5 quanta is the one with the highest probability. That this is not always the case can be seen from Figures 6.17, 6.18, and 6.19, in which similar results are represented for $\Theta=110$, 150, and 170°, respectively. As one goes from small to large $\Theta$, the probability of exciting the CO stretch by a double collision mechanism becomes smaller at the same time that the probability of exciting the slow modes, represented by v=0, becomes larger by the same mechanism. This trend could be explained if one tries to visualize the trajectory of a double collision with a large scattering angle. Such a trajectory would be one in which the projectile had suffered a very small deflection by the adsorbate so that it would strike the metal surface with a very small angle of incidence. Consequently, considering an almost flat surface, the projectile would be deflected

by the surface into a large scattering angle. According to this argument, the double collision peak would be mainly due to the slow modes of the metal surface. The fact that the single collision peak almost disappears in going from θ=100 to θ=170° seems to suggest that the modes with E symmetry in the cluster have higher probabilities of excitation than the modes with A symmetry, giving lower DDCS for larger scattering angles. The total DDCS obtained by summing over all n is shown in Figure 6.20 as a function of ε and θ. The same trend observed in the individual contributions is seen here.

Results obtained for the bridge model are not much different than the ones obtained for the top, although some differences can be pointed out. In the bridge model at θ=180°, the excitation of CO stretch by n=5 and n=6 have almost the same probabilities. Additionally, the peaks in the bridge model appear to be wider than in the case of the top model. This can be a consequence of the larger number of modes considered as slow modes in the bridge model. In Figure 6.22 a comparison of the DDCS summed over all n for the two models is presented for θ=180°. It is found that the bridge model gives smaller DDCS than the top model. The effect of the temperature is shown in Figure 6.23 where the DDCS summed over all n are presented for a temperature of 100° K. As in the case of scattering by He atoms, the width of the peaks decreases when decreasing the temperature. The effect seems to be more noticeable for the single collision peak than for the double collision one.

Figure 6.1a Single (----) and double (- - -) collision contribution to the partial double differential cross-sections at scattering angles $\Phi$=0, $\Theta$=100, for n=0 CO molecules adsorbed on top.

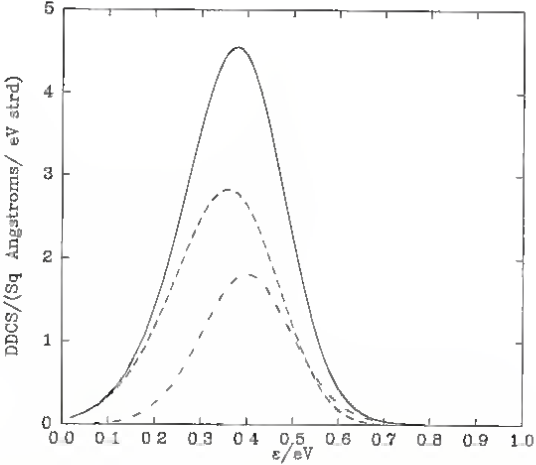
DDCS/(Sq Angstroms/ eV strd)
0
1
2
3
4
5
0.0
0.1
0.2
0.3
0.4
0.5
0.6
0.7
0.8
0.9
1.0
ε/eV

Figure 5.2: Single ( --) and double (- - -) collision contributions to the partial double differential cross-sections at scattering angles $\phi=0$, $\theta=100$ for $n=0$ CO molecule adsorbed on bridge site.

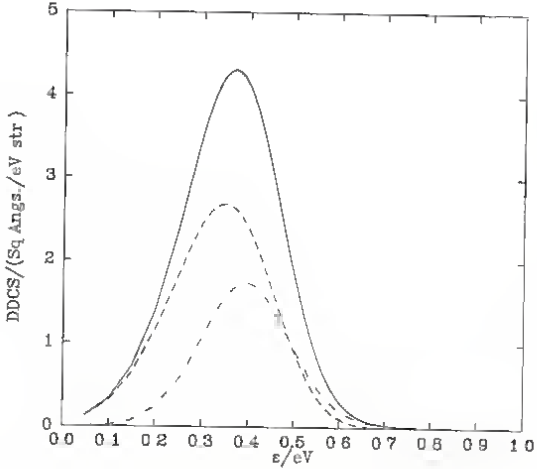
DDCS/(Sq Angs./eV str )
ε/eV
0
1
2
3
4
5
0.0
0.1
0.2
0.3
0.4
0.5
0.6
0.7
0.8
0.9
1.0

Figure 6.3 Single (---) and double (– – –) collision contributions to the partial double differential cross-sections at angles $\theta_2=0$, $\theta_1=100$, for excitation of CO stretch by $n=1$

DDCS/(Sq. Angstroms/ eV strd)
2.0
1.5
1.0
0.5
0.0
0.0 0.1 0.2 0.3 0.4 0.5 0.6 0.7 0.8 0.9 1.0
ε/eV

Figure 6.4: Single (---) and double (- - -) collision contributions to the partial double differential cross sections at angles $\phi=0$, $\theta=100$, for excitation of CO stretch by $n=2$.

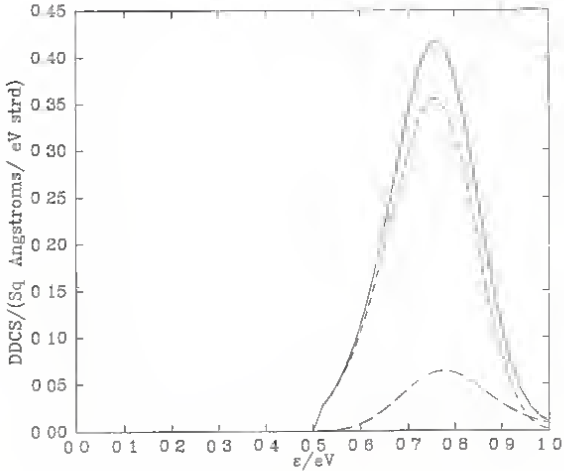
DDCS/(Sq Angstroms/ eV strd)
0.45
0.40
0.35
0.30
0.25
0.20
0.15
0.10
0.05
0.00
0.0 0.1 0.2 0.3 0.4 0.5 0.6 0.7 0.8 0.9 1.0
ε/eV

Figure 6.5: Excitation of the CO stretch by n quanta, tep model. Scattering angles θ=90, θ=140, T=300 k, E=1 eV

DDCS x 10/(Sq.Ange/eV str)
10
8
6
4
2
0
0
1
2
3
4
E/eV

Figure 6.6: Excitation of the CO stretch by n quanta, bridge model. Scattering angles $\theta_i$=140, T=300 k, E=1 eV.

DDCS x 10/(Sq Angs/eV str)
10
8
6
4
2
0
0
1
2
3
4
-h-
2
4
6
8
E = 15 eV

Figure 6 7: He DDCS for CO stretch excitation by n=0,1,2 and 3 quanta. Top (——) and bridge (– – –) models. θ=100°, T=300 K

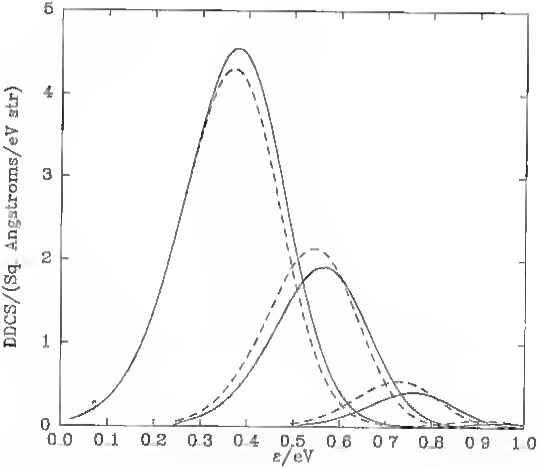
DDCS/(Sq. Angstroms/eV str)
0
1
2
3
4
5
0.0
0.1
0.2
0.3
0.4
0.5
0.6
0.7
0.8
0.9
1.0
ε/eV

Figure 6-8: He DDCS for CO stretch excitation by n=0,1,2 and 3 quanta. Top (——) and bridge (– – –) models. θ=140°, T=300 K.

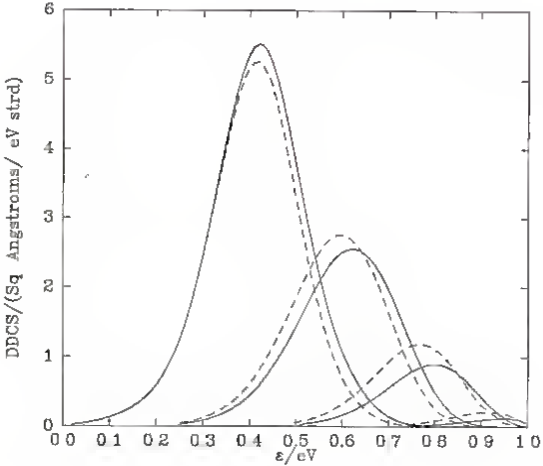
DDCS/(Sq Angstroms/ eV strd)
0
1
2
3
4
5
6
0 0 0 1 0 2 0 3 0 4 0 5 0 6 0 7 0 8 0 9 1 0
ε/eV

Figure 6_9 He DDCS for CO stretch excitation by $\Delta n$=0,1,2 and 3 quanta. Top (——) and bridge (– – –) models. $\theta$=170°, T=300 K

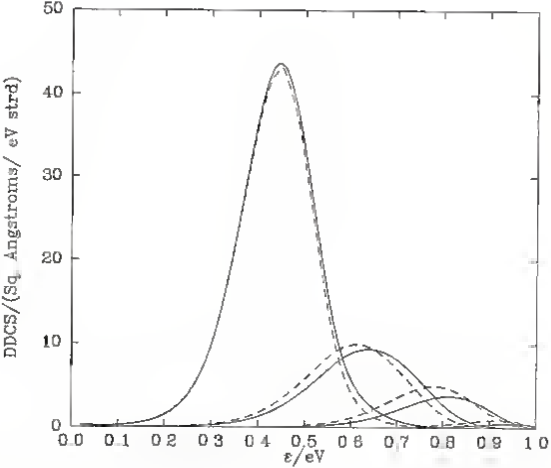
DDCS/(Sq. Angstroms/ eV strd)
50
40
30
20
10
0
0.0 0.1 0.2 0.3 0.4 0.5 0.6 0.7 0.8 0.9 1.0
ε/eV

Figure 6.10: He DDCS for CO stretch excitation by -n=0,1,2 and 3 quanta. Top (——) and bridge (– – –) models. Θ=100°, T=100 K.

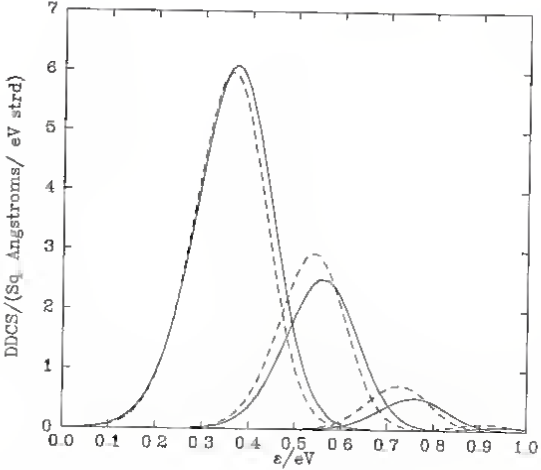
DDCS/(Sq. Angstroms/ eV strd)
7
6
5
4
3
2
1
0
0.0 0.1 0.2 0.3 0.4 0.5 0.6 0.7 0.8 0.9 1.0
ε/eV

Figure 6 11: He DDCS for CO stretch excitation by n $O_2$ 1,2 and 3 quanta. Top (——) and bridge (– – –) models. $\theta$=140°, T=100 K

DDCS/(Sq. Angstroms/ eV strd)
0
1
2
3
4
5
6
7
8
0.0 0.1 0.2 0.3 0.4 0.5 0.6 0.7 0.8 0.9 1.0
ε/eV

Figure 6.12 He DDCS for CO stretch excitation by $n=0,1,2$ and 3 quanta. Tap (——) and bridge (– – –) models $\theta=170°$, $T=100$ K.

DDCS/(Sq Angstroms/ eV strd)
70
60
50
40
30
20
10
0
0.0 0.1 0.2 0.3 0.4 0.5 0.6 0.7 0.8 0.9 1.0
E/eV

Figure 6.13: He DDCS in the region of very small energy transfers for T=100 K and θ=170°.

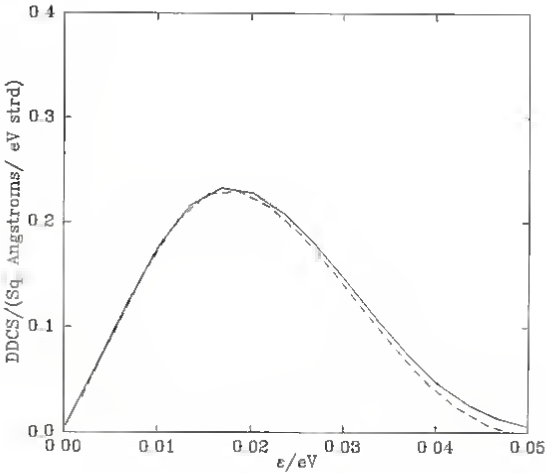
0.4
0.3
0.2
0.1
0.0
DDCS/(Sq. Angstroms/ eV strd)
0.00
0.01
0.02
0.03
0.04
0.05
ε/eV

Figure 5.14 He DDCS summed over n for $\theta$=100°. Top model.

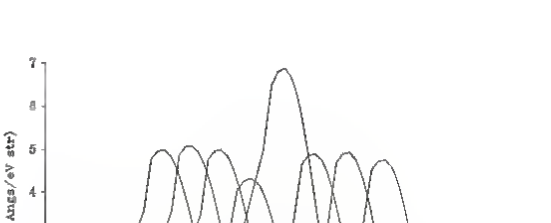
DDCS /(Sq Angs/eV str)
7
6
5
4
3
2
1
0
e x 10
e
0
2
4
6
8
10
φ x θ 1/deg

Figure 6.15 Re DDCS summed over u for $\theta = 100°$. Bridge model.

DDCS /(Sq.Am2s/eV str)
10
8
6
4
2
0
0
2
4
6
8
10
θ x 0.1/deg
ε 10 eV
20

Figure 6.16: $Li^+$ ODCS for excitation of the CO stretch by n quanta, Top model $E_i$=10 eV, T = 300 K, $\theta$=100, $\phi$=0°.

DDCS x10 /(Sq.Angs/eV str)
10
8
6
4
2
0
0
4
8
12
16
n
4
8
$\Delta E$ =

Figure 6 17: $Li^+$ DDCS for excitation of the CO stretch by n quanta. Top model, $E_i$=10 eV, T=300° K, $\theta$=110 $\phi$=0.

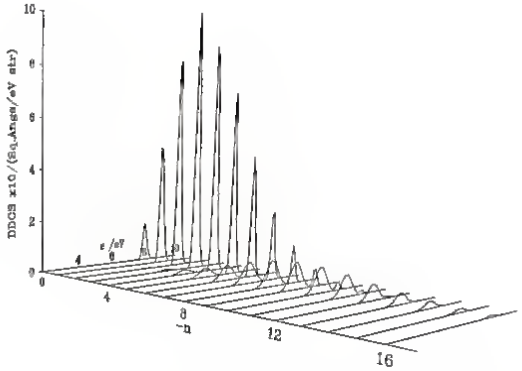
DDCS x10/(Sq.Angs/eV str)
10
8
6
4
2
0
ε /eV
0
4
8
12
16
-h

Figure 6 18 $Li^+$ DDCS for excitation of the CO stretch by $n$ quanta Top model, E=10 eV T=300° K, $\theta$=150, $\phi$=0.

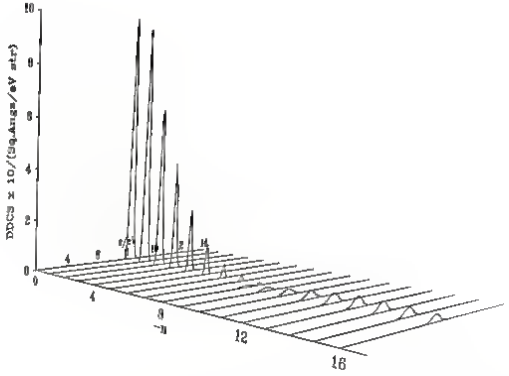
DDCS x 10/(Sq.Angs/eV str)
0
2
4
6
8
10
4
8
12
16

Figure 6.19 $Li^+$ DDCS for excitation of the CO stretch by n quanta. Top model, E=10 eV, T=300° K, $\theta$=170, $\Phi$=0

DDCS x1D /(En Amps/eV str)
10
8
6
4
2
0
0
4
8
12
16
n-
ε (eV)

Figure 6.20: $Li^+$ DDCS (summed over n) E=10 eV, $\Phi$=0°, T=300° K, top model

DDCS x 10/(Sq.Angs/eV str)
10
8
6
4
2
0
10
12
14
16
18
θ x 0.1/deg
ε /eV
4
6
8
10

Figure 6.21 $Li^+$ DDCS for excitation of the CO stretch by n quanta. E=10 eV, $\theta$=100°, $\phi$=0°, T=300° K Bridge model

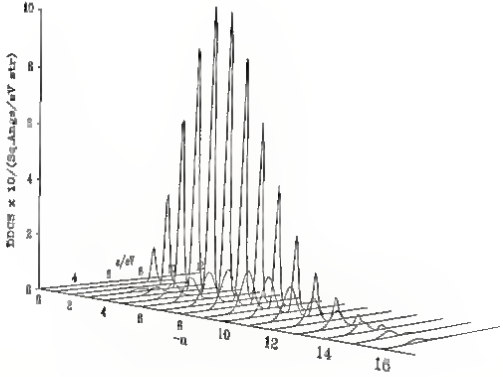
DDCS x 10/(Sq.Angs/eV str)
0
2
4
6
8
10
e/eV
-a
12
14
16

Figure 6.22: $Li^+$ DDCS (summed over n) Top (——) and bridge (– – –) model. E=10 eV, T=0.0° K, $\phi$=0, $\theta$=100.

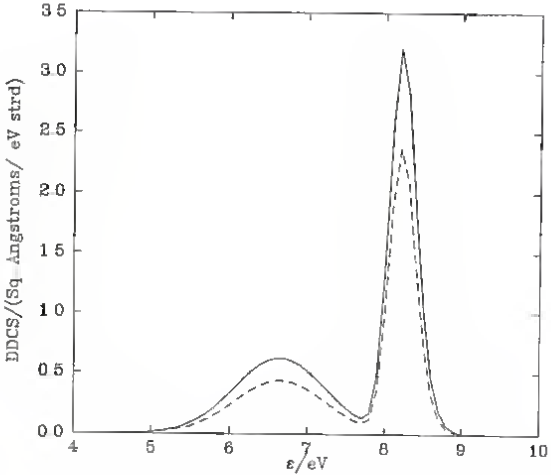
3.5
3.0
2.5
2.0
1.5
1.0
0.5
0.0
DDCS/(Sq. Angstroms/ eV strd)
4
5
6
7
8
9
10
ε/eV

Figure 6.23 Li$^+$ DDCS (summed over n). Top (——) and bridge (– – –) model E=10 eV, T=100° K, Φ=0, Θ=100.

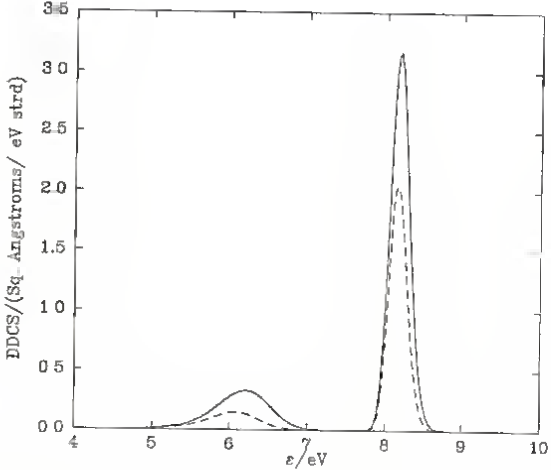
DDCS/(Sq. Angstroms/ eV strd)
3.5
3.0
2.5
2.0
1.5
1.0
0.5
0.0
4
5
6
7
8
9
10
ε/eV

# CHAPTER 7

## SUMMARY AND CONCLUSIONS

In this work we have presented a theoretical model suitable for the study of scattering of atoms or ions with hyperthermal energies by molecules adsorbed on metal surfaces at low coverages. A simple model to obtain the vibrational modes of molecules adsorbed on surfaces has been presented and frequencies have been calculated for a CO molecule adsorbed on a Ni(001) surface. The procedure allows for the modelling of different adsorption sites and makes the classification of the modes according to symmetry an easy task.

An interaction potential has been constructed and a trajectory study of the elastic scattering of He atoms and $Li^+$ ions by a CO molecule adsorbed on a metal surface has been carried out. It is found that at the hyperthermal energies of 1 eV for He atoms and of 10 eV for $Li^+$ atoms, the effective classical cross-sections for the adsorbed molecule-surface complex do not show the corrugation of the surface to a great extent and, in the case of $Li^+$ ions, the image potential effect is almost negligible except around polar scattering angles of $\pi/2$.

We have obtained double differential cross sections as functions of energy transfer, scattering angles, incident energy and metal temperature for the cases of a CO molecule adsorbed either at the bridge or on-top configuration.

The approach we have followed allows us to predict which excitation process is the most likely to occur at a given scattering angle and for a certain energy transfer. For example, we are able to predict that in the scattering of He atoms, the most likely energy loss would be found at 0.4 eV and would be due to a collective excitation of modes with lower frequencies and not to the excitation of the CO stretch mode. We could also say that features found at large transfer of energy would most likely correspond to multiple excitations of the CO stretch of the adsorbed molecule.

From the temperature effect, we can say that more information on the excitation of individual modes can be obtained by performing experiments at lower temperatures where features of the low frequency modes such as hindered rotations and translations would be enhanced.

Related to this point, we would like to mention that in an experimental study of He scattered by CO molecules (Lahee, et al.) at low CO coverages on a Pt(001) surface, a peak at 6.0 meV was attributed to CO vibrations. Another very weak structure was seen at 16.5 meV and was assigned to the hindered rotation. This assignment was based on the results of some calculations (Richardson and Bradshow) that have given a value of 22.5 meV for this mode. However, in our calculations of the vibrational modes we obtained values for the frustrated rotations for the bridge and top models, of 15.5 and 16.2 meV, respectively. These values are very close to the one measured in the experiments. Furthermore, as was discussed in Chapter 6, in our calculations for DDCS, we obtain a very weak peak centered at about 17 meV for both models. We believe this peak should correspond to the frustrated rotations on either model.

The results obtained for the scattering of $Li^+$ ions suggest that a more complicated process occurs in comparison with the He case. For one thing, double collisions seem to play a major role in the process. Although excitations of the CO stretch involve large numbers of quanta that are added up, they give results where predictions can be made. For example, one can predict that most of the energy loss peaks should be found at large energy transfers. One can also say that, depending on the scattering angle, one can expect to find either a single peak at large values of transferred energy or two peaks, one broad and at lower values of transferred energy and another narrow peak centered at larger values of transferred energy.

In order to obtain more information about the individual modes, a more detailed calculation, where more modes are specified by the quantum numbers $n_j$, is needed. This can be readily obtained from our approach when the short time expansion approximation is only used for a few modes. For example, the bridge site, where the distinction between high and low frequency modes is not so sharp, could be treated in this way.

A more rigorous treatment of double and multiple collisions can be based on the multiple scattering expansion of the transition operator and can be developed within the time-correlation formalism.

One obvious limitation in our model is that it ignores the large number of low-frequency bulk vibrational modes of the substrate. These modes could in principle be obtained with the standard methods of lattice dynamics, and have actually been used in the problem of adsorbate vibrations (Rahman et al., 1982). However, these methods can be applied to molecular adsorbates with great difficulty and

since they rely on lattice periodicity their application to disordered systems is even more complex

A possible method which could be used to deal with this limitation, but would still have the convenience of a cluster model, consists of including periodic boundary conditions for the clusters Periodicity in the directions parallel to the crystal surface is accomplished by adding new bond-stretching internal coordinates, in additional to the ones within the cluster, between edge atoms located on opposite sides of a layer in the crystal and between edge atoms on two adjacent layers of the crystal This method would provide modes with well defined values of the momentum parallel to the surface, allowing thus to examine the dispersion of the mode frequency and the energy transfer into these modes as a function of the parallel momentum This method have been used to generate the spectra of the O/Ni(001) system (Lloyd and Hemminger, 1985) and found to reproduce almost exactly the results obtained with the Green's function lattice dynamics technique However in our treatment we consider hyperthermal energies which are dominated by short-time dynamics and these modes are not likely to have an effect in the process

Another aspect of the model that needs attention is the assumption of harmonicity One of the most interesting aspects associated with the vibrational states of chemisorbed molecules is the change in vibrational frequencies and lifetime of a molecule upon adsorption One of the mechanisms which give rise to the shift and broadening of the vibrational state of a chemisorbed molecule on a metal surface is vibrational energy relaxation This mechanism is associated with the coupling between the localized vibrational modes of the adsorbated and the phonon modes of the metal The

effectiveness of this mechanism depends of the anharmonicity of the potential and also on the frequency of the localized vibrational mode in relation to the highest phonon frequency of the metal. By analogy with the study of multiphonon processes in the bulk (Mills et al., 1980) one may infer that for modes with frequencies greater than twice the highest phonon frequency of the metal the damping provided by anharmonic processes would be very weak. On the other hand, for low-frequency modes, such as the C-Ni stretching vibration for CO adsorbed on a Ni(001) surface, decay via two-phonon emission is energetically possible and probably the relevant energy relaxation process. Again because of the short time dynamics in hyperthermal collisions this effect can be ignored.

If necessary, at low collision energies, anharmonicity can be introduced in the formalism of the time correlation functions for adsorbates on metal surfaces along the same lines as it is done in the case of polyatomics (Wijnaendts and Micha, 1983b).

In a general way one can write the vibrational potential in terms of a harmonic part, $V_h$, and an anharmonic one $V_a$, such that in terms of the normal coordinates that diagonalize the harmonic part of the vibrational Hamiltonian, the total vibrational Hamiltonian is given by

$$H_v = H_h + V_a(Q) ,$$

$$H_h = (\underline{P}^T\underline{P} + \underline{Q}^T\underline{\omega}_h^2\underline{Q})/2 ,$$

where $\underline{P}$ is the column matrix of momenta $P_i = -i\hbar\partial/\partial Q_i$. One then finds that the TCFs are given in terms of displacement-displacement correlation functions (DDCS), $\langle\langle \underline{Q}(0)\ \underline{Q}^T(t)\rangle\rangle$ which can be evaluated from the corresponding double-time Green functions. The procedure

involves the introduction of a set of time independent parameters, $\underline{\lambda}$, which relates to the harmonic frequencies, $\underline{\omega}_h$, and the new effective anharmonic ones $\bar{\omega}$ by the equation $\underline{D}^T(\underline{\omega}_h^2 - \underline{\lambda})\underline{D} = \bar{\omega}^2$ with $\underline{D}^T\underline{D} = \underline{1}$ and the anharmonic frequencies $\omega$ can be obtained from their relation with the DDCS, that is

$$M\bar{\omega}\coth\underline{u} = 2\underline{D}^T\underline{V}\underline{D} ,$$

$$\underline{V} = \langle\langle\underline{Q}\,\underline{Q}^T\rangle\rangle\,\underline{\omega}_h^2 - \langle\langle\underline{Q}\,\underline{F}^T\rangle\rangle ,$$

where $\underline{u} = M\bar{\omega}/(2k_B T)$ and $\underline{F}$ is the column matrix of the anharmonic forces that act on the $Q_j$. The vibrational correlation function can then be given by the expression

$$F_v(\vec{R},t) = \prod_{j=1}^{N_v} \exp[-X_j \coth\bar{u}_j +$$

$$+ X_j\{\exp(-\alpha_j \quad i\bar{\omega}_j t) + \exp(\alpha_j + i\bar{\omega}_j t)\}/2\} ,$$

where $X_j = h(\vec{R}\,\underline{\xi}_j)^2/(2\bar{\omega}_j \sinh\bar{u}_j)$ ,

and $\bar{\underline{\xi}} = \underline{\xi}\,\underline{D}$

This expression is similar to the one obtained from harmonic motions but the vibrational probabilities now depend on the anharmonic forces

In order to study the scattering of atoms by adsorbates at thermal energies, a semi-classical approach could be used. Within a semi-classical model, the intermolecular potential $V(t)=V(\vec{R}(t), r^N)$ depends on the motion of the projectile relative to the center of mass of the target. Furthermore, $V(t)$ is an operator that acts on the internal states of the target. During a collision, an internal

state of the target, $|\alpha>$, evolves in time in accordance with the semiclassical Hamiltonian $H(t)$, so that the probability for a transition between an initial state, $|\alpha>$, and a final one, $|\alpha'>$, is given by

$$W_{\alpha'\alpha} = \lim_{t\to\infty} \frac{1}{t} |<\alpha'|\alpha,t>|^2$$

To evaluate this probability, one can separate the time evolution of $|\alpha,t>$ into a part that corresponds to the motion of the non-interacting parts, that is, the projectile and the target, and another that contains the intermolecular forces. To achieve this separation one works in the interaction picture and writes

$$|\alpha,t> = \exp[-iH_i(t-t_i)/\hbar]\ U(t,t_i)\ |\alpha,t_i>$$

where

$$H_i = \lim_{t\to-\infty} H(t)$$

and $U(t,t_i)$ is the time evolution operator in the interaction representation. Using this expression of $|\alpha,t>$ in the expression for the transition probability $W_{\alpha|\alpha'}$ one obtains

$$W_{\alpha'\alpha} = |<\alpha'|\hat{U}(\infty,-\infty)|\alpha>|^2$$

This quantity can then be used to obtain the differential probability of energy transfer, $\varepsilon$, from an initial state $|\alpha>$ to a final one $|\alpha'>$. This is found to be given by

$$\frac{d\mathcal{P}_{\alpha}}{d\varepsilon} = \sum_{\alpha'} W_{\alpha'\alpha}\ \delta[\varepsilon - (E_{\alpha'} - E_{\alpha})]$$

This equation can be expressed in terms of a time correlation function with the final result given by

$$dP/d\varepsilon = \int_{-\infty}^{\infty} dt/2\pi\hbar \; F(t) \exp( i\varepsilon t/\hbar)$$

where

$$F(t) = \langle\langle U_X^{\dagger}(0) \; U_X(t)\rangle\rangle$$

and

$U_X(t)$ is given by

$$U_X(t) = \exp(iH_X t/\hbar) \; U(\infty, -\infty) \exp(iH_X t/\hbar)$$

so that the differential probability of energy transfer is given by the Fourier transform of the TCF of the semiclassical evolution operator. Then the procedure to follow will involve first defining the Hamiltonian of the non-interacting parts, and next obtaining $\dot{U}(t,t_1)$. This requires the integration of the differential equation of the evolution operator, that is

$$[i\hbar\partial/\partial t - H^{-}(t,t_1)] \; U(t,t_1) = 0$$

with

$$U(t,t) = 1$$

and

$$H^{-}(t,t_1) = \Delta K(t) + \exp[1(Hi(t-t_1)/\hbar] \; V(t) \exp[-iH_i(t-t_1)/\hbar]$$

where

$$\Delta K(t) = [\vec{P}^2(t) - \vec{P}_i^2]/(2M)$$

$\vec{P}$ being the initial relative momentum. This approach would provide the means to tackle the problem of scattering of atoms at thermal energies by adsorbates

As one can see collisional TCFs are of general validity, and can be used in conjunction with approximations proved to be valid in special cases. Several aspects of the approach that we have presented can be developed in future work. In particular, in view of the increasing amount of experimental work currently in progress on the scattering of atoms at thermal energies, it would be fruitful to look into the semiclassical method.

The approach proposed in this work in its present form could be applied without major changes to different systems. Calculations could be done for example for a different crystal face of the same metal or any other metal, or for a different type of adsorbed molecule and even for a different type of projectile. Also, calculations could be done for incident angles different from zero. The case of higher coverages could also be studied with the present approach, including the interaction between the adsorbates.

APPENDIX A
COEFFICIENTS FOR THE TRANSFORMATION $\underline{s} = A\underline{X}$

a) On-Top Cluster

$s_{12} = X_{Ni}$

$s_{13} = -Y_{Ni}$

$s_{14} = -s_{12}$

$s_{15} = -s_{13}$

$s_{16} = -(X_{Ni} + Y_{Ni})/2 + \sqrt{2}\ Z_{Ni}/2$

$s_{17} = -(X_{Ni} - Y_{Ni})/2 + \sqrt{2}\ Z_{Ni}/2)$

$s_{18} = (X_{Ni} + Y_{Ni})/2 + \sqrt{2}\ Z_{Ni}/2)$

$s_{19} = (X_{Ni} - Y_{Ni})/2 + \sqrt{2}\ Z_{Ni}/2$

$s_{CNi} = Z_C - Z_{Ni}$

$s_{CO} = Z_O - Z_C$

$s_a = X_C + Y_C - (X_O + Y_O)/d_{CO} - (X_{CNi} + Y_{CNi})/d_{CNi}$

$s_b = (X_{Ni} + Y_{Ni})/d_{CNi} - (X_C + Y_C)/d_{CNi}$

b) Bridge Cluster

$s_{13} = (2/\sqrt{5}\ x_{Ni}^{(1)} - (1/\sqrt{5})\ Y_{Ni}^{(1)}$

$s_{14} = -Y_{Ni}^{(1)}$

Appendix A (continued)

$$s_{15} = (2/\sqrt{5})\, x_{Ni}^{(1)} - (1/\sqrt{5})\, y_{Ni}^{(1)}$$

$$s_{12} = y_{Ni}^{(1)} - y_{Ni}^{(2)}$$

$$s_{26} = -(2/\sqrt{5})\, x_{Ni}^{(2)} + (1/\sqrt{5})\, y_{Ni}^{(2)}$$

$$s_{27} = y_{Ni}^{(2)}$$

$$s_{28} = (2/\sqrt{5})\, x_{Ni}^{(2)} + (1/\sqrt{5})\, y_{Ni}^{(2)}$$

$$s_{19} = (1/\sqrt{3})\, x_{Ni}^{(1)} + (\sqrt{2/3})\, z_{Ni}^{(1)}$$

$$s_{1,10} = (1/\sqrt{7})\, x_{Ni}^{(1)} - (2/\sqrt{7})\, y_{Ni}^{(1)} + (\sqrt{2/7})\, z_{Ni}^{(1)}$$

$$s_{1,11} = -(1/\sqrt{7})\, x_{Ni}^{(1)} - (2/\sqrt{7})\, y_{Ni}^{(1)} + (\sqrt{2/7})\, z_{Ni}^{(1)}$$

$$s_{1,12} = -(1/\sqrt{3})\, x_{Ni}^{(1)} + (\sqrt{2/3})\, z_{Ni}^{(1)}$$

$$s_{2,9} = (1/\sqrt{3})\, x_{Ni}^{(2)} + (\sqrt{2/3})\, z_{Ni}^{(2)}$$

$$s_{2,12} = -(1/\sqrt{3})\, x_{Ni}^{(2)} + (\sqrt{2/3})\, z_{Ni}^{(2)}$$

$$s_{2,13} = -(1/\sqrt{7})\, x_{Ni}^{(2)} + (2/\sqrt{7})\, y_{Ni}^{(2)} + (\sqrt{2/7})\, z_{Ni}^{(2)}$$

$$s_{2,14} = (1/\sqrt{7})\, x_{Ni}^{(2)} + (2/\sqrt{7})\, y_{Ni}^{(2)} + (\sqrt{2/7})\, z_{Ni}^{(2)}$$

$$s_{CO} = z_O - z_C$$

$$s_{CNi(1)} = (d_{Ni}/2d_{CNi})(y_{Ni}^{(1)} - y_C) + (d_C/d_{CN_i})(z_C - z_{Ni}^{(1)})$$

$$s_{CNi(2)} = (d_{Ni}/2d_{CNi})(y_C - y_{Ni}^{(2)}) + (d_C/d_{CN_i})(z_C - z_{Ni}^{(2)})$$

$$s_a = (d_C/d_{CNi}^2)(y_{N_i}^{(2)} - y_{N_i}^{(1)}) + 2[(d_C^2 + d_{CNi}^2)/(d_{Ni}d_{CN_i}^2)](z_{Ni}^{(1)} + z_{Ni}^{(2)})$$

$$+ [d_C/(d_C^2 + d_{Ni}^2) - 1/d_{CO}]\, z_C - 2(d_C/d_{Ni}\, d_{CO})\, z_O$$

$$s_b = (2/d_{CNi})(X_{Ni}^{(1)} + X_{Ni}^{(2)}) - (4/d_{CNi})\, X_C$$

$$s_d = (d_C/d_{CNi}^2)(Y_{Ni}^{(1)} - Y_{Ni}^{(2)}) + (d_{Ni}/d_{CNi}^2)(Z_{Ni}^{(1)})(Z_{Ni}^{(2)})$$

$$s_g = -(1/2d_C)(X_{Ni}^{(1)} + X_{Ni}^{(2)}) + [(d_C + d_{CO})/(d_C\, d_{CO})]\, X_C \quad (1/d_{CO})\, X_O$$

## APPENDIX B
## SYMMETRY ADAPTED COORDINATES

a) On-Top Cluster

$$S_1^{A_1} = Z_{Ni}^{(1)}$$

$$S_2^{A_1} = Z_C$$

$$S_3^{A_1} = Z_O$$

$$S_4^{E} = (X_{Ni} + Y_{Ni})/\sqrt{2}$$

$$S_5^{E} = (X_C + Y_C)/\sqrt{2}$$

$$S_6^{E} = (X_O + Y_O)/\sqrt{2}$$

b) Bridge Cluster

$$S_1^{A_1} = Z_C$$

$$S_2^{A_1} = Z_O$$

$$S_3^{A_1} = (Z_{Ni}^{(1)} + Z_{Ni}^{(2)})/\sqrt{2}$$

$$S_4^{A_1} = (Y_{Ni}^{(1)} - Y_{Ni}^{(2)})/\sqrt{2}$$

$$S_5^{E_1} = X_C$$

$$S_6^{E_1} = X_O$$

$$S_7^{E_1} = (X_{Ni}^{(1)} + X_{Ni}^{(2)})/\sqrt{2}$$

$$S_8^{E_2} = Y_C$$

$$S_9^{E_2} = Y_O$$

$$S_{10}^{E_2} = (Y_{Ni}^{(1)} + Y_{Ni}^{(2)})/\sqrt{2}$$

$$S_{11}^{E_2} = (Z_{Ni}^{(1)} - Z_{Ni}^{(2)})/\sqrt{2}$$

$$S_{12}^{A_2} = (X_{Ni}^{(2)} - X_{Ni}^{(1)})/\sqrt{2}$$

APPENDIX C
COEFFICIENTS FOR TRANSFORMATION $O_{\alpha\beta}=C_{\alpha i}^{\dagger}$

a) On-Top Cluster

| | $X_{Ni}$ | $Y_{Ni}$ | $Z_{Ni}$ | $X_C$ | $Y_C$ | $Z_C$ | $X_O$ | $Y_O$ | $Z_O$ |
|---|---|---|---|---|---|---|---|---|---|
| $O_1^{A_1}$ | 0 | 0 | 0.025 | 0 | 0 | -0.778 | 0 | 0 | 0.628 |
| $O_2^{A_1}$ | 0 | 0 | 0.602 | 0 | 0 | -0.490 | 0 | 0 | -0.631 |
| $O_2^{A_1}$ | 0 | 0 | 0.798 | 0 | 0 | 0.393 | 0 | 0 | 0.456 |
| $O_4^{E}$ | 0.135 | 0.135 | 0 | -0.622 | 0.622 | 0 | 0.308 | 0.308 | 0 |
| $O_5^{E}$ | 0.692 | 0.692 | 0 | 0.093 | 0.093 | 0 | 0.115 | -0.115 | 0 |
| $O_6^{E}$ | 0.061 | 0.061 | 0 | 0.323 | 0.323 | 0 | 0.626 | 0.626 | 0 |

Appendix C (continued)

b) Bridge Cluster

| | $X_{Ni}(1)$ | $Y_{Ni}(1)$ | $Z_{Ni}(1)$ | $X_{Ni}(2)$ | $Y_{Ni}(2)$ | $Z_{Ni}(2)$ | $X_C$ | $Y_C$ | $Z_C$ | $X_O$ | $Y_O$ | $Z_O$ |
|---|---|---|---|---|---|---|---|---|---|---|---|---|
| $O_1^A1$ | 0 | 0.007 | -0.001 | 0 | -0.007 | -0.001 | 0 | 0 | 0.758 | 0 | 0 | -0.653 |
| $O_2^A1$ | 0 | -0.559 | 0.296 | 0 | -0.559 | -0.296 | 0 | 0 | 0.258 | 0 | 0 | 0.344 |
| $O_3^A1$ | 0 | 0.428 | 0.301 | 0 | -0.428 | 0.301 | 0 | 0 | 0.444 | 0 | 0 | -0.507 |
| $O_4^A1$ | 0 | -0.065 | 0.568 | 0 | 0.065 | -0.568 | 0 | 0 | -0.385 | 0 | 0 | -0.446 |
| $O_5^B1$ | -0.146 | 0 | 0 | 0.146 | 0 | 0 | 0.935 | 0 | 0 | -0.287 | 0 | 0 |
| $O_6^B1$ | -0.672 | 0 | 0 | 0.672 | 0 | 0 | -0.122 | 0 | 0 | 0.286 | 0 | 0 |
| $O_7^B1$ | 0.165 | 0 | 0 | 0.165 | 0 | 0 | 0.332 | 0 | 0 | 0.917 | 0 | 0 |

Appendix C (continued)

| | $X_{Ni}(1)$ | $Y_{Ni}(1)$ | $Z_{Ni}(1)$ | $X_{Ni}(2)$ | $Y_{Ni}(2)$ | $Z_{Ni}(2)$ | $X_C$ | $Y_C$ | $Z_C$ | $X_O$ | $Y_O$ | $Z_O$ |
|---|---|---|---|---|---|---|---|---|---|---|---|---|
| $O_5^{B_2}$ | 0 | 0.013 | 0.405 | 0 | 0.013 | -0.405 | 0 | 0.239 | 0 | 0 | 0.784 | 0 |
| $O_9^{B_2}$ | 0 | 0.443 | 0.299 | 0 | 0.443 | -0.299 | 0 | 0.484 | 0 | 0 | 0.441 | 0 |
| $O_{10}^{B_2}$ | 0 | 0.549 | 0.260 | 0 | 0.549 | -0.260 | 0 | 0.333 | 0 | 0 | 0.388 | 0 |
| $O_{11}^{B_2}$ | 0 | -0.037 | 0.424 | 0 | -0.037 | -0.424 | 0 | -0.773 | 0 | 0 | 0.200 | 0 |
| $O_{12}^{A_2}$ | 0.707 | 0 | 0 | 0.707 | 0 | 0 | 0 | 0 | 0 | 0 | 0 | 0 |

## REFERENCES


Allison, J N , and W A Goddard (1982), Surface Sci , 115, 551

Andersson, S , (1977), in : 3rd Int. Conf. on Solid Surfaces, Vienna

Andersson, S , and J B Pendry (1979), Phys Rev Letters, 43, 363

Andersson, S., and J.B. Pendry (1980), J. Phys., C13, 3547

Annett, J F., and R Haydock (1984) Phys Rev Lett., 53, 838

Batra I P , P S Bagus, and J A Barker (1985), Phys Rev , B31, 1737

Bauschlicher, C W , P S Bagus, C.J Nelin, and B O Ross (1986), J Chem Phys, 85, 354

Berndt R., J P. Toennies and Ch Wöll (1987), Abstract to the 5th International Congress on Vibrations at Surfaces, Gramau-Erbsee, Germany

Bertolini, J C , and B Tardy (1981), Surface Sci., 102, 131.

Block, J.H., (1982), Surface Sci , 116, 240

Block, J E , P Bopp, K Lutzenkirchen, and H Wolfberg (1982), J Chem , Phys., 76, 6431.

Block, J E , O A Campbell, and R F Wallis (1981), Surface Sci , 105, 629

Clary, D.C. (1982), Chem Phys , 65, 247

Clouthier, D J , and D A Ramsay (1983), Ann Rev Phys Chem , 34, 31

Crawford, B L , and A Horwitz (1948), J Chem Phys., 16, 147

Englert, W , E Taglauer, W Heiland and D P Jackson (1983). Physica Scripta, T6, 38

Eshjerg N , and J.K Norskov (1980), Phys Rev Lett , 45, 807

Gadzuk, J W (1987) in: Vibrational Spectroscopy of Molecules on Surfaces, eds , J T Yates and T E Madey, Plenum Press, New York

Gentry, W R (1979), in: Atom-Molecule Collision Theory, ed R.B. Bernstein, Plenum Press, New York

Gerber, R.S., A T. Yinon, and R Kosloff (1984), Chem Phys Lett 105, 523

Goldberger, M L , and K M Watson (1964), Collision Theory, Wiley, New York

Goldstein, H (1950), Classical Mechanics, Addison-Wesley: Cambridge

Goodman, F A (1987), J Chem. Phys. 58, 5530.

Harris, J , and A. Liebsch (1982a), J Phys C15, 2275

Harris, J., and A Liebsch (1982b), Phys Rev Lett , 49, 341.

Herzberg, G. (1945), Spectra of Diatomic Molecules, D von Nostrand Co., New York.

Hulpke E. (1975), Surface Sci 52, 615.

Hulpke, E., and K. Mann (1985), Surface Sci , 157, 245

Ibach, H., and D L Mills (1982), Electron Energy Loss Spectroscopy and Surface Vibrations, Academic, New York

Ibañez, J., M Garcia, and J M Rojo (1983), Phys. Rev , B28, 3164.

Jonee, L.H (1960), J. Mol Spectrosc., 5, 133

Jonsson, H., J.H. Weare, and A.C Levi (1984), Surface Sci , 148, 126

Lahee, A M., J R Manson, and J P Toennies, Ch Woll (1987), J. Chem. Phys., 86, 7194.

Lehwald, S , and H. Ibach (1982), in: Vibrations at Surfaces, ed by R. Gaudano, J.M. Gilles, A A Lucas, Plenum, New York

Levi, A.C. (1982), in: Dynamics of Gas-Surface Interaction, eds. G Manedek and V. Balbusa, Springer, Berlin

Liu, W K , and E. Gumbalter (1987), Surface Sci , 180, 169.

Lloyd, K G , and J.C Messinger (1985), J. Chem Phys , 82, 3858.

Mann, K , V Celli, and J.P Toennies (1987), Surface Sci , 185, 269.

Messiah, A. (1961), Quantum Mechanics, Vol 1, North Holland, Amsterdam

Micha, D A (1979a), J Chem Phys , 70, 565

Micha, D.A. (1979b), J. Chem Phys., 70, 3165.

Micha, D A (1981), J Chem Phys , 74, 2054.

Micha, D A (1986), Intern J Quantum Chem , 2D, 773

Mills, D L , C J Duthler, and M Sparks In: Disordered Solids, Optical Properties, Dynamical Properties of Solids, vol 4, eds G K Horton, and A A Maradudin, North Holland, Amsterdam

Perre, Z , and D A Micha (1986), Chem Phys Letters, 132, 488

Poelsema, B , R L Palleer, S T De Zwart and G Comsa (1983), Surface Sci , 126, 641

Rahman, T S , J E Black, and D L Mills (1982), Phys Rev , B25, 883

Rahman, T S , D L Mills, and J E Black (1983), Phys Rev , B27, 4059

Richardson, N V , and A M Bradshev (1979), Surface Sci , 88, 255

Rocca, M , M Ibach, S Lehwald, and T S Rachman (1986), In: Structure and Dynamics of Surfaces I, eds W Schommers and P von Blanckenhagen, Springer Verlag, Berlin

Rodberg, L S , and R M Thaler (1967), in: Introduction to the Quantum Theory of Scattering, Academic Press, New York

Shampine, L F , and M K Gordon (1975), Computer Solution of Ordinary Differential Equations: The Initial Value Problem, Freeman, San Francisco

Singh, M , D K Darol, and H Rabitz (1986), J Chem Phys , 84, 1373

Steele, W A, (1974), The Interaction of Gases with Solid Surfaces, Pergamon Press, Oxford

Strong, R L , B Firey, G W de Wette, and J L Erskine (1982), Phys Rev , B26, 3483.

Tenner A D , K T Gillen, T G M Horn, J Lee, and A W Kleyn (1986), Surface Sci., 172, 90

Van Hove, L (1954), Phys Rev , 95, 249

Villalonga, E , and D A Micha (1983a), J Chem Phys , 78, 3942

Villalonga E , and D A Micha (1983b), J Chem Phys , 79, 3794

Villalonga E , and D A Micha (1987) J Chem Phys , 87, 750

Villalonga, E., and H Rabitz (1986), J Chem Phys , 85, 2300.

Willis, R F. (1980), in: Vibrational Spectroscopy of Adsorbates, Springer, Berlin

Wilson, E.B., J.C. Decius, and P.C. Cross (1955), Molecular Vibrations, McGraw-Hill, New York.

Zaremba, E., and W. Kohn (1977), Phys. Rev., B15, 1769

BIOGRAPHICAL SKETCH

Zaide Parra was born in Maracay, Venezuela, on August 3, 19[illegible]. She attended school in Venezuela and received her Licenciado in Chemistry from the University of the Andes, Merida, Venezuela, in July of 1976. From September of 1976 until February of 1980 she was employed as Instructor of Chemistry at the University of the Andes. She was promoted to her present position as Assistant Professor in February 1980. In February of 1981 she was awarded a fellowship to study for the Ph.D. degree at the University of Florida's Quantum Theory Project, where she has been until the present. In August of 1983, she attended the Summer Institute in Quantum Theory in Uppsala, Sweden.

I certify that I have read this study and that in my opinion it conforms to acceptable standards of scholarly presentation and is fully adequate, in scope and quality, as a dissertation for the degree of Doctor of Philosophy

David A. Micha, Chairman
Professor of Chemistry and Physics

I certify that I have read this study and that in my opinion it conforms to acceptable standards of scholarly presentation and is fully adequate, in scope and quality, as a dissertation for the degree of Doctor of Philosophy.

John R. Eyler
Professor of Chemistry

I certify that I have read this study and that in my opinion it conforms to acceptable standards of scholarly presentation and is fully adequate, in scope and quality, as a dissertation for the degree of Doctor of Philosophy.

Willis B. Person
Professor of Chemistry

I certify that I have read this study and that in my opinion it conforms to acceptable standards of scholarly presentation and is fully adequate, in scope and quality, as a dissertation for the degree of Doctor of Philosophy.

Henk J. Monkhorst
Professor of Physics and Chemistry

I certify that I have read this study and that in my opinion it conforms to acceptable standards of scholarly presentation and is fully adequate, in scope and quality, as a dissertation for the degree of Doctor of Philosophy.

Samuel B. Trickey
Professor of Physics and Chemistry

This dissertation was submitted to the Graduate Faculty of the Department of Chemistry in the College of Liberal Arts and Sciences and to the Graduate School, and was accepted as partial fulfillment of the requirements for the degree of Doctor of Philosophy.

August, 1968

Dean, Graduate School